Landfill Gas Distribution at the Base of Passive Methane Oxidation Biosystems: Transient State Analysis of Several Configurations

Bahar Ahoughalandari [a] and Alexandre R. Cabral [a,*]

[a] Geoenvironmental Group, Department of Civil Engineering, University of Sherbrooke, Sherbrooke, Quebec, Canada J1K 2R1.

[*] Corresponding author: Tel.: +1 819 821-7906. Postal address: 2500, boul. de l'Université, Sherbrooke, Quebec, Canada J1K 2R1.

E-mail addresses: alexandre.cabral@usherbrooke.ca (A. R. Cabral); bahar.ahou@usherbrooke.ca (B. Ahoughalandari)

Waste Management 69 (2017) 298–314

ARTICLE INFO

Article history:
Received 4 November 2016
Revised 9 August 2017
Accepted 13 August 2017
Available online 18 August 2017

Keywords:
Passive methane oxidation biosystems
Numerical simulation
Unsaturated hydraulic behavior
Landfill final covers
Design
Landfill gas flow

* Corresponding author at: 2500, boul. de l'Université, Sherbrooke, Quebec J1K 2R1, Canada.
E-mail addresses: bahar.ahou@usherbrooke.ca (B. Ahoughalandari), alexandre.cabral@usherbrooke.ca (A.R. Cabral).

http://dx.doi.org/10.1016/j.wasman.2017.08.027

Abstract

The design process of passive methane oxidation biosystems needs to include design criteria that account for the effect of unsaturated hydraulic behavior on landfill gas migration, in particular, restrictions to landfill gas flow due to the capillary barrier effect, which can greatly affect methane oxidation rates. This paper reports the results of numerical simulations performed to assess the landfill gas flow behavior of several passive methane oxidation biosystems. The concepts of these biosystems were inspired by selected configurations found in the technical literature. We adopted the length of unrestricted gas migration (LUGM) as the main design criterion in this assessment. LUGM is defined as the length along the interface between the methane oxidation and gas distribution layers, where the pores of the methane oxidation layer material can be considered blocked for all practical purposes. High values of LUGM indicate that landfill gas can flow easily across this interface. Low values of LUGM indicate greater chances of having preferential upward flow and, consequently, finding hotspots on the surface. Deficient designs may result in the occurrence of hotspots. One of the designs evaluated included an alternative to a concept recently proposed where the interface between the methane oxidation and gas distribution layers was jagged (in the form of a see-saw). The idea behind this ingenious concept is to prevent blockage of air-filled pores in the upper areas of the jagged segments. The results of the simulations revealed the extent of the capability of the different scenarios to provide unrestricted and conveniently distributed upward landfill gas flow. They also stress the importance of incorporating an appropriate design criterion in the selection of the methane oxidation layer materials and the geometrical form of passive biosystems.

Keywords: Passive methane oxidation biosystems; Numerical simulation; Unsaturated hydraulic behavior; Landfill final covers; Design; Landfill gas flow

1. Introduction

Passive methane oxidation biosystems (PMOBs), which include certain types of biofilters, biowindows and biocovers that are not operated by active ventilation or other means of control, have been the focus of numerous studies in recent years. PMOBs may be constructed in the upper layers of a final cover system, in the absence of or in combination with active collection systems of landfill gas. They consist of two main layers: the gas distribution layer (GDL) and the methane oxidation layer (MOL). The gas distribution layer serves to maximize the spatial distribution of landfill gas, originating either from the underlying waste body or from a gas supply pipe, to the methane oxidation layer. The methane oxidation layer is located at the surface and is where methanotrophic bacteria oxidize CH_4 into CO_2 in the presence of molecular O_2. Several environmental parameters control the rate of methane oxidation in PMOBs, including the texture of the methane oxidation layer materials, temperature, NH_4^+ and NO_3^- contents, presence of vegetation, etc. (e.g. Chanton et al. 2011; He et al. 2012; Huber-Humer et al. 2008; Scheutz et al. 2009; Spokas and Bogner 2011).

Regardless of the mechanism of gas flow, i.e. advection or diffusion, moisture is another key parameter affecting methane oxidation rates, because it controls gas flow behaviour through unsaturated soils (e.g. Fredlund et al. 2012; Langfelder et al. 1968; Lu and Likos 2004; Tang et al. 2011). The specific influence of soil moisture on the methane oxidation rate in a particular soil depends on its water retention characteristics and therefore varies with soil texture and degree of compaction. When the moisture content is low enough, gas is free to migrate by diffusion in the air phase or – if the pressure is high enough – by advection. When cracks are formed and the landfill gas is under pressure, gas flows mainly by advection.

However, when the moisture content (or degree of saturation) increases and reaches a certain value, the upward flow of CH_4 and downward flow of O_2 through the methane oxidation layer would be greatly reduced (Adu-Wusu and Yanful 2006; Bussière et al. 2003; Cabral et al. 2010). A point may be reached where the air phase is no longer continuous and gas molecules have to diffuse in the liquid phase, which significantly slows down the process. Indeed, the coefficient of diffusion of oxygen through a saturated or nearly saturated layer is approximately four orders of magnitude lower than in air (Cabral et al. 2000; Yanful 1993). This may result in concentrated loadings at the base of the methane oxidation layer, which may lead to concentrated flow, therefore unacceptable surface CH_4 concentrations, i.e. hotspots (Rachor et al. 2013; Rower et al. 2011). Moisture accumulation in the methane oxidation layer is partly related to the capillary barrier effect along the interface between the gas distribution and methane oxidation layers (Ahoughalandari and Cabral 2017; Tétreault et al. 2013). The capillary barrier effect is formed when a fine-textured soil overlies a coarser one. The contrasts in textural and hydraulic properties between the moisture retention layer (upper layer) and the capillary break layer (bottom layer) lead to moisture retention above the interface.

The usual concept employed in many passive methane oxidation biosystems is that of a sloped plane interface between the methane oxidation and gas distribution layers. Tétreault et al. (2013) performed steady-state numerical simulations based on estimated parameters of an experimental site in Germany and another in the Netherlands, both with sloped plane interfaces. Tétreault et al.'s (2013) results showed that the capillary barrier effect led to high degrees of saturation along most of the GDL-MOL interface. Consequently, landfill gas would be diverted towards the usually drier upslope area of these experimental plots, which has indeed been reported by Geck et al. (2012; 2016) and Röwer et al. (2012).

In order to overcome the problems posed by sloped plane interfaces, Cassini et al. (2017) proposed an ingenious concept where a series of jagged-shaped segments form the GDL-MOL interface. An experimental plot was constructed according to this concept at the AV Miljø landfill, Denmark. The idea behind the peculiar geometric concept was to ensure that landfill gas would migrate unrestricted at least in the upper part of each segment, where moisture would be low. Higher moisture content values – and possibly pore blockage by the presence of water – would be limited to the lower parts of each segment. Unrestricted refers herein to a pronounced reduction in gas flux due to the presence of water (moisture) in the pores. Considering the problem of landfill gas migration in passive methane oxidation biosystems, restriction to flow due to the presence of solid particles is disregarded. In a formal design procedure, the length of the unrestricted part of each segment would have to be calculated using appropriate design parameters, to maximize methane oxidation, and minimize hotspot formation.

In fact, most experimental plots – with jagged or sloped plane interfaces – have not been conceived following a formal design process. When this is the case, the potential restriction to landfill gas migration across the GDL-MOL interface should be assessed following clear design criteria, based on hydraulic parameters and other plausible concerns. Ahoughalandari (2016) suggested a single design criterion to incorporate the capillary barrier effect in the design of PMOBs. This criterion was denominated the length of unrestricted gas migration (LUGM). As illustrated in Figure 1, this PMOB is characterized by a capillary barrier between the methane oxidation and gas distribution layers. LUGM is defined as the length along the interface between the methane oxidation and gas distribution layers where the pores of the methane oxidation layer material are filled with water to the extent where, for all practical purposes, they can be considered blocked to gas flow.

Figure 1 Schematic defenition of the length of unrestricted gas migration (LUGM)

Ahoughalandari (2016) proposed a design parameter that allows obtaining the value of the design criterion, i.e. LUGM. The proposed design parameter is the volumetric air content associated with the threshold of unrestricted gas migration, $\theta_{a\text{-}occ}$, which can be obtained using – preferably – the air permeability function of the candidate methane oxidation layer material. Alternatively, the water retention curve or Standard Proctor curve of the methane oxidation layer material can be used. Several studies show that the degree of water saturation associated with the line of optima of the Standard Proctor curve corresponds to that associated with the occlusion of air-filled pores, i.e. $\theta_{a\text{-}occ}$ (Ahoughalandari 2016; Jucá and Maciel 2006; Langfelder et al. 1968; Marinho et al. 2001). This is attributed to the fact the pores of soils compacted on the wet side of optimum are in the form of discontinuous bubbles, whereas the air phase is continuous on the dry side of optimum (Leroueil and Hight 2013). For materials where there is a gradual decrease in degree of water saturation in the vicinity of the air entry value and for which the air entry value is not well defined, it is possible to obtain the degree of water saturation associated with $\theta_{a\text{-}occ}$ using the degree of saturation associated with the air entry value (Ahoughalandari 2016; Jucá and Maciel 2006; Springer et al. 1998). In addition, according to Ahoughalandari (2016), the greater the horizontal distance between the isolines of the degree of water saturation on the Standard Proctor curve and the steeper the slope of the desaturation zone on water retention curve, the steeper the slope of ka-functions where $\theta_a > \theta_{a\text{-}occ}$ or $\theta_a >$ conservative $\theta_{a\text{-}occ}$. Details of the methodology to obtain $\theta_{a\text{-}occ}$ are provided in Ahoughalandari (2016). Ahoughalandari and Cabral (2017) evaluated the influence of several geometric and hydraulic parameters on the distribution of landfill gas at the base of the

134 methane oxidation layer using LUGM as the design criterion: the smaller the value of LUGM,
135 the smaller the region along the interface where gas could migrate unrestricted. The chances
136 of having high surface CH_4 concentration, i.e. hotspots, would increase accordingly.

137 In the present study, transient-state numerical simulations were performed to assess the
138 relative ease of landfill gas migration at the base of the methane oxidation layer of two PMOB
139 configurations, all inspired from the technical literature (Cassini et al. 2017; Ndanga et al.
140 2015). The design parameters associated with the methane oxidation layer materials were
141 identified, and the value of LUGM was obtained for each case. The quality of different
142 designs was assessed solely based on LUGM, therefore in terms of the landfill gas flow at the
143 base of the methane oxidation layer.

144 The main limitations of the present study are two-fold: the first is related to the lack of
145 consideration of evapotranspiration in the numerical simulations, and, indirectly, the
146 importance of plant roots or vegetation in moisture release or retention. This limitation was
147 circumvented by considering seepage rates (the flux of water that reached the top of the
148 PMOB) as a percentage of the total precipitation. This percentage was assumed equal to that
149 found by Cabral et al. (2010) for a reasonably similar cover design, constructed in the same
150 landfill. The second limitation relates to the lack of consideration of water generation due to
151 biotic activity. Evaluation of the moisture changes due to biotic activity is beyond the scope
152 of this paper.

153 Future PMOBs should be designed following a robust process that includes consideration of
154 unsaturated flow, such as presented herein. This is key to the adoption of PMOBs in the
155 reduction of total greenhouse gas emissions from landfills.

156

157 ## 2. Material and methods

2.1. Site configurations and associated materials

2.1.1. *Modified Danish concepts 1* and *2*

The *modified Danish concept* 1 was based on an experimental PMOB (12 m × 42 m) built in the AV Miljø landfill, Denmark (Cassini et al. 2017). The configuration of this concept included an 80 to 90-cm-thick methane oxidation layer and a gas distribution layer of variable thickness (30-50 cm). Figure 2a presents a 3-D view of this concept, whereas Figure 2b shows the cross section of the PMOB along the West-East axis, where the interface is jagged (in the form of a "zig-zag", as Cassini et al. (2017) called it). Along the width of the PMOB, i.e. the North-South axis (Figure 2c), the interface is a horizontal plane with the gas distribution layer becoming thicker to accommodate the gentle slope perpendicular to the jagged interface.

Considering the formation of a capillary barrier between the gas distribution and methane oxidation layers, part of each segment (near the top) of the jagged interface (Figure 2b) was assumed to provide a permanent unrestricted channel for upward landfill gas flow (where moisture would be low enough), whereas the bottom parts might become restricted – permanently or not - due to higher moisture levels.

In the simulations presented herein, the slope of the jagged interface and the width of each segment were equal to 15% and 2 m, respectively (Figure 2b). The slope of the base of the gas distribution layer was assumed equal to 3% (Figure 2b). In the *modified Danish concept 2,* we considered the width of each segment equal to 4 m (an arbitrary value), while the slope of the base of the gas distribution layer was arbitrarily kept at 3%. The schematic representation of *modified Danish concept 2* is similar to the *modified Danish concept 1.*

Figure 2: (a) 3D view; (b) representative segment along the West-East direction; and (c) section view along the North South direction of the *modified Danish concepts*

Compost and coarse gravel were used to construct the methane oxidation and the gas distribution layers, respectively. For the simulations presented herein we adopted the properties of the sand-compost and gravel used to construct the methane oxidation and gas distribution layers of an experimental PMOB constructed at the St-Nicephore landfill, Quebec, Canada (Capanema and Cabral 2012). The sand-compost mixture was a mixture of five volumes of compost and one volume of coarse sand (D_{10} = 0.07 mm, D_{85} = 0.8 mm, and the coefficient of uniformity (C_u = 4.3), organic matter content (f_{OC}) equal to 17.8% $g_{o\text{-}m}/g_{dry\text{-}soil}$, specific gravity equal to 2.24, optimum gravimetric water content and maximum dry density (Standard Proctor) equal to 43% and 1080 kg/m^3, respectively.

The drying water retention curve of the sand-compost mixture was obtained using HYPROP apparatus (UMS 2013) (Figure 3a). The sample was compacted at dry density similar to the in situ value (750 kg/m^3). For the gas distribution layer, the water retention curve (Figure 3a) was estimated using the Fredlund et al. (2002) model, derived from the grain size distribution curve of the material. The water retention curve describes the relationship between matric suction and volumetric water content (or degree of saturation), and its shape is mainly influenced by the pore size distribution. For practical purposes, the water retention curve may be modelled using continuous functions (e.g. the van Genuchten (1980) model), or may be estimated using equations based on grain size distribution curve (e.g. the Fredlund et al. (2002) model).

The saturated hydraulic conductivity (k_{sat}) of the sand-compost (9×10^{-6} m/s) was obtained according to ASTM D2434-68 (2006). The k_{sat} of the gas distribution layer was calculated

204 using the Chapuis (2004) equation. The van Genuchten (1980) model, based on the Mualem
205 formulation (1976), was used to obtain the hydraulic conductivity functions of all materials in
206 Figure 3b.

207

208 Figure 3: (a) Water retention curves; and (b) hydraulic conductivity functions, used in
209 simulations of the *modified Danish concepts* and *alternative Danish concept*

210

211 **2.1.2.** ***Alternative to Danish concept***

212 An alternative concept is proposed herein based on the Danish concept. In this case, the
213 geometric concept of the *modified Danish concept 1* was altered so that the jagged interface
214 remained the same, but the interface along the North-South axis (the width of the PMOB)
215 followed a 5% slope (Figure 4a). In addition, the thickness of the gas distribution layer
216 remained constant (Figure 4a and c; North-South direction). The methane oxidation layer was
217 subdivided into two layers: a 15-cm layer of sand-compost mixture and a 45-60 cm layer of
218 fine sand (Figure 4b and c). This choice of materials to constitute the *alternative Danish*
219 *concept* was based on the fact that very high methane oxidation efficiencies were obtained by
220 Ndanga et al. (2015) when using this combination of materials, both in laboratory-scale
221 column experiments and experimental field plots.

222

223 Figure 4: (a) 3D view; (b) representative cross section along the West-East direction; and (c)
224 section view along the North South direction of the *alternative Danish concept*

225

226 The material used to construct the gas distribution layer was similar to the gravel used in the
227 *modified Danish concepts*, and the same compost material adopted in the *modified Danish*
228 *concepts* was used for the 15-cm layer of sand-compost mixture (Figure 4). The material of
229 the 45-60 cm layer of fine sand was composed of a uniform sand (D_{50} = 0.15 mm and C_u =
230 2.25) with specific gravity equal to 2.71, optimum water content ~ 12.0%, and maximum dry
231 density equal to 1750 kg/m^3. Using the HYPROP apparatus (UMS 2013), the drying water
232 retention curve of fine sand (Figure 4a) was obtained at initial dry density equal to 1650
233 kg/m^3. This arbitrary value was selected because it was the actual dry density value of a field
234 experiment with this material. The k_{sat} of fine sand was calculated using the Chapuis (2004)
235 equation, and its hydraulic conductivity function (Figure 4b) was obtained using the van
236 Genuchten (1980) model, based on the Mualem formulation (1976).

237 A summary of the hydraulic properties of the materials used in numerical simulations is
238 presented in Table 1, where k_{sat} is the hydraulic conductivity, θ_s is saturated volumetric water
239 content, θ_r is residual volumetric water content, *a* and *n* are experimental parameters in the .
240 van Genuchten (1980) model.

241

242 Table 1: Hydraulic properties of the materials used in numerical simulations

243 The cover profile and associated materials for an additional configuration (*German*
244 *configuration*) are provided as Supplementary Materials. This configuration is based on a
245 large-scale experimental PMOB (20 m × 30 m) with a slope of 1 Vertical:10 Horizontal
246 (1V:10H), where the presence of a hotspot near the upslope edge was observed during the
247 field investigation (personal communication during a site visit with Sonja Bohn, who was
248 responsible for the investigations on this experimental PMOB; see also Tétreault et al.
249 (2013)).

2.2. Design criteria and design parameters for unrestricted flow of landfill gas at the base of the methane oxidation layer

In PMOBs, the methane oxidation layer often acts as the moisture retention layer of the capillary barrier and the gas distribution layer acts as the capillary break layer. In order to consider the influence of the capillary barrier effect on upward flow of landfill gas across the GDL-MOL interface of PMOBs, Ahoughalandari (2016) suggested adopting LUGM as design criterion and the volumetric air content at the threshold of occlusion to gas migration, $\theta_{a\text{-}occ}$, as the design parameter. If the volumetric air content, θ_a, in the methane oxidation layer - at the GDL-MOL interface - is greater than $\theta_{a\text{-}occ}$, we propose herein to assume that gas can flow unrestrictedly. Otherwise, it is considered that the air phase is occluded by water (i.e. air-filled voids are no longer interconnected), and that gas can only migrate by molecular diffusion in the liquid phase.

For the sake of considering the influence of the capillary barrier effect in gas flow behavior of PMOBs, the values of θ_a in the moisture retention layer of each capillary barrier, obtained close to the interface, had to be compared to the design parameter, $\theta_{a\text{-}occ}$. The value of $\theta_{a\text{-}occ}$ is ideally obtained using the air permeability function (k_a-function), as illustrated in Figure 5a. Alternatively, the water retention curve and/or the Standard Proctor curve of the MOL material can be employed, if the k_a-function is not available (Ahoughalandari 2016). The air permeability function describes how the coefficient of air permeability (or of the gas intrinsic permeability) varies with the volumetric air content, volumetric water content, moisture content, degree of saturation, or suction. It is presented herein in the form of a relationship between the gas intrinsic permeability and volumetric air content. The gas intrinsic

permeability can be obtained following ASTM D6539-13 (2006), employed herein with slight modifications (details in Ahoughalandari 2016).

While $\theta_{a\text{-}occ}$ can be easily identified in Figure 5a (θ_a where k_a drops abruptly), there are cases where the k_a-function does not show an abrupt fall in k_a. In such cases, there is a transition zone, as illustrated in Figure 5b, and we suggest adopting a volumetric air content value (θ_a) lower than $\theta_{a\text{-}occ}$. A practical denomination for this design parameter is **conservative** $\theta_{a\text{-}occ}$, identified in Figure 5b. In fact, in numerical simulations with SEEP/W, the parameters that are actually compared are the volumetric water content in the methane oxidation layer along the interface, θ_w, and the volumetric water content associated with $\theta_{a\text{-}occ}$, i.e. $\theta_{w\text{-}occ;}$ or their associated **conservatives**. SEEP/W simulates numerically the real physical process of water flowing through porous media.

2.2.1. *Modified Danish concepts*

The capillary barrier effect between the sand-compost mixture (i.e. moisture retention layer) and gravel (i.e. capillary break layer) for the *modified Danish concepts* is operational (water is blocked at the interface) as long as $\psi_i > 4.50$ kPa. Since the k_a-function of the sand-compost mixture was obtained in the laboratory, the values of the design parameters could be defined precisely. The **conservative** $\theta_{a\text{-}occ}$ was determined to be at the onset of the transition zone on the k_a-function of the sand-compost (ellipse in Figure 5b), i.e. **conservative** $\theta_{a\text{-}occ} \approx 16\%$. Assuming that the dry density was equal to the in situ value, i.e. 750 kg/m^3, the **conservative** $\theta_{w\text{-}occ}$ is therefore equal to 50.5%.

Figure 5: Gas intrinsic permeability function and the design parameter for (a) fine sand used in the simulations of the *alternative Danish concept* ; and (b) sand-compost used in the simulations of *modified Danish concepts* and *alternative Danish concept*

$LUGM_{cg}$ is defined at each segment and the final LUGM for this particular design is the sum of all $LUGM_{cg}$ values. $LUGM_{cg}$ is the length along the interface within a segment, taken horizontally, for which θ_a > **conservative** $\theta_{a\text{-}occ}$ in the sand-compost (Figure 2b). Considering the fact that the control variable during numerical simulations with SEEP/W was the volumetric water content, the value of $LUGM_{cg}$ was the length along the interface within a segment, taken horizontally, along which θ_w at the interface was lower than the **conservative** $\theta_{w\text{-}occ}$ in the sand-compost.

The geometric features of the interfaces along the length and width of the *modified Danish concepts* are not the same (Cassini et al. 2017). This can be clearly observed in the 3D views and cross sections presented in Figure 2. Therefore, two other types of LUGM need to be defined in the direction perpendicular to the jagged interface (North-South) of the *modified Danish concepts* (Figure 2c). $LUGM_{MG1\text{-}pr}$ is the length along the MG1 interface (top of a segment; Figure 2c) between the sand-compost and gravel layers, taken horizontally, where θ_w < **conservative** $\theta_{w\text{-}occ}$ in the sand-compost. $LUGM_{MG2\text{-}pr}$ is similar, but measured along the bottom of each segment (MG2 interface; Figure 2c). This distinction is necessary when evaluating suction and moisture content values during numerical simulations, because differences in potential energies result in different elevation heads and, consequently in different suction and volumetric water content values.

2.2.2. *Alternative Danish concept*

319 This concept was developed following analysis of the behaviour of the PMOBs modelled
320 according to the two modified Danish concepts. To increase the value of LUGM, we added
321 another layer. In this case, a capillary barrier is created between the sand-compost mixture
322 (moisture retention layer) and the fine sand (capillary break layer) layers and the capillary
323 barrier effect is operational insofar as $\psi_i > 50$ kPa. A second capillary barrier is created
324 below the first capillary barrier. This second barrier is made up of fine sand over gravel, and
325 is operational for $\psi_i > 1.30$ kPa.

326 The design parameter value for the fine sand, $\theta_{a\text{-}occ}$, was equal to approximately 9%. It was
327 selected using its experimental k_a-function (Figure 5a). The values of gas intrinsic
328 permeability in the k_a-function were obtained using a flow meter connected to the triaxial
329 apparatus. More details with this regard can be found in Ahoughalandari (2016). $\theta_{w\text{-}occ}$ was
330 calculated using the initial dry density of the fine sand (1650 kg/m3) and is equal to 30%. The
331 design parameter value for the sand-compost layer was the same as in the *modified Danish*
332 *concepts*.

333 For each interface of the lowest capillary barrier within the *alternative Danish concept* (fine
334 sand - gravel), $LUGM_{tot}$ is the summation of the individual $LUGM_{fg}$ (Figure 4b), i.e. the
335 length along the interface between the fine sand layer and gas distribution layer, taken
336 horizontally, until θ_w is greater than the $\theta_{w\text{-}occ}$ (Figure 4b). In the case of the upper-most
337 (horizontal) capillary barrier, $LUGM_{cf}$ is the length along the interface between the
338 sand-compost and fine sand layers until θ_w is greater than the **conservative** $\theta_{w\text{-}occ}$ within the
339 sand-compost (Figure 4b).

340 Along the width of the *alternative Danish concept*, three other design criteria (LUGM) need
341 to be defined: The first is $LUGM_{cf\text{-}pr}$, which is the length along the interface between the
342 sand-compost layer and fine sand layer, taken horizontally from upslope until the point where

343 θ_w is greater than the **conservative** $\theta_{w\text{-}occ}$ in the sand-compost (Figure 4c). The second is
344 $LUGM_{FG1\text{-}pr}$, which is the length along the FG1 interface, i.e. between the fine sand layer and
345 gas distribution layer along the top of the jagged segment (Figure 4c), taken horizontally,
346 from the top of the sloping interface, until the point where volumetric water content is lower
347 than $\theta_{w\text{-}occ}$ in the fine sand (Figure 4c). The last and third is $LUGM_{FG2\text{-}pr}$, which is similar to
348 $LUGM_{FG1\text{-}pr}$, but taken along the bottom of the jagged FG2 interface (Figure 4c). As in the
349 previous case, the distinction between top and bottom interfaces is necessary because their
350 different elevations lead to different elevation heads, suction values and moisture content
351 values for the same distance from the top (measured horizontally).

352

353 **2.3. Numerical simulations**

354 In order to perform the numerical simulations, the finite element software SEEP/W 2007
355 (GEO-SLOPE 2010) was used. SEEP/W simulates the unsaturated/saturated flow of water
356 through a porous medium using the Richards equations (2016). In the simulations presented
357 herein, the lengths of all PMOBs were equal to 50 m. The widths of the *modified* and
358 *alternative Danish concepts* were considered equal to 20 m. The mesh was denser near the
359 interfaces. The geometric features of the interface and the thicknesses of the constituting
360 layers followed the configurations described in section 2.1. The finite element mesh pattern
361 was triangular with approximate global element size equal to 0.07 m. Depending on the
362 geometry of the modeled PMOB, the number of elements varied from 24500 to 25500.

363 Two types of boundary conditions were considered in the simulations: 1) *unit flux function* to
364 assign the seepage reaching the top of the PMOB, and 2) *zero total flux* boundary condition
365 with *potential seepage face review* to simulate the drainage systems. The boundary conditions
366 adopted for the simulations are provided as Supplementary Materials (Figure S-1).

In the case of the *modified Danish concepts* and the *alternative Danish concept*, considering the different shapes of the interfaces along the North-South and the West-East directions and the fact that SEEP/W is limited to 2D analysis, the following simulations were performed: 1) along the West-East direction; 2) along the North-South direction, i.e. along the MG1 and FG1 interfaces (Figure 2a and Figure 4a); and 3) along the North-South direction, i.e. along the MG2 and FG2 interfaces (Figure 2a and Figure 4a).

All numerical simulations were performed under transient state and lasted 246 days (therefore 246 steps in SEEP/W) for the *modified and alternative Danish concepts*. Since SEEP/W cannot account for evapotranspiration, we decided to use seepage rates, i.e. the flux of water reaching the top of the PMOB. In the present case, we applied the seepage rate value found by Cabral et al. (2010) for a similar experimental cover, i.e. 22% of the total precipitation. Since we modeled under transient state, the actual seepage value varied with time. SEEP/W also does not allow for inclusion of moisture changes due to biotic activity; therefore, the latter was also not considered. For the *modified Danish concepts* precipitation data for St-Nicephore, Quebec was considered. The daily seepage rates for the three cases are presented in Figure 6. The total annual precipitation in this site is approximately 1100 mm.

Figure 6: Daily seepage rate into *Modified and alternative Danish concepts* (using data for Quebec, Canada)

The initial θ_w in the sand-compost mixture for the *modified Danish* and *alternative Danish concepts* were equal to 45%, while the initial θ_w for the fine sand (*alternative Danish concept*) was 16%. All these initial values of θ_w were assigned using the "activation PWP" option in SEEP/W, by which the pore water pressure value associated with each initial value of θ_w was

391 introduced as the initial condition for each given material. Several other initial conditions
392 were tested, but the one adopted led to faster and more reliable convergence of iterative
393 calculations by SEEP/W.

394

395 3. Results and Discussion

396 The θ_w values presented in all figures were obtained from the nodes located 1 cm above or
397 below each interface. Due to boundary condition effects near the extremities of the models,
398 only θ_w values sufficiently far from them were considered in the analyses. Accordingly,
399 values associated with points within 1 m from the upslope extremity and 5 m from the
400 downslope extremity were not considered. In addition to the results presented herein, we
401 present the results pertaining to the *German configuration* as Supplementary Materials.

402

403 *3.1. Modified Danish concepts*

404 Figure 7 presents the θ_w values in the sand-compost layer (i.e. methane oxidation layer), along
405 the GDL-MOL interface of one segment, and the evolution of $LUGM_{cg}$ (defined in Figure 2)
406 in the *modified Danish concept 1* (West-East direction). Since the segments are constructed
407 on a horizontal surface, the same pattern of distribution and evolution of θ_w along the jagged
408 interfaces and the same value of $LUGM_{cg}$ were obtained for all segments (data not presented).

409

410 Figure 7: Evolution and distribution of (a) θ_w in the methane oxidation layer along the
411 GDL-MOL interface, and (b) $LUGM_{cg}$ - *modified Danish concept 1*, West-East direction

412

On Day 136, the θ_w values of the points located on the lower part of the segment started to exceed the **conservative** $\theta_{w\text{-}occ}$ for the sand-compost (i.e. 50.5%). On Day 145, all the θ_w values were greater than the **conservative** $\theta_{w\text{-}occ}$. The difference between the maximum and minimum values of θ_w along the interface, which represents the level of uniformity and is referred to as $\Delta\theta_w$, increased with time. The maximum value of $\Delta\theta_w$ was equal to 2.9% and occurred on Day 199, when the interface was completely restricted to gas migration. The magnitude of this maximum $\Delta\theta_w$ indicates that the moisture distribution was rather uniform.

Figure 7b shows the evolution of $LUGM_{cg}$ in the *modified Danish concept 1*. On Day 136, $LUGM_{cg}$ started to decrease gradually, and on Day 145 it was equal to zero. Indeed, from Day 136 until Day 145 the jagged form of the interface helped to keep the interface partially unrestricted near the top of the segment, while the bottom parts were restricted. During the last 101 days of the simulation, $LUGM_{cg}$ was equal to zero. This total restriction was partly caused by the several rainy events that occurred during and previous to Day 145 (see Figure 6b), which led to moisture accumulation at the interface.

These results seem to indicate that the sand-compost used as the methane oxidation layer would not be able to provide the minimum permanently unrestricted passages for upward flow of landfill gas at the top of each segment of the *modified Danish concept 1*. This is associated with several factors, including the low drainage capacity of the sand-compost mixture (MOL material), the potential formation of a capillary barrier at the interface (which depends on the contrast of hydraulic permeability of the methane oxidation and gas distribution layers), the daily seepage rate, and the available time duration for draining the sand-compost mixture. The geometrical features of the biosystem (slope, thickness of layers, etc.) also play an important role.

Figure 8: Distribution and evolution of θ_w in the sand-compost along (a) the MG1 interface, and (b) the MG2 interface of the *modified Danish concept 1*, North-South direction

Figure 8 shows the θ_w values in the sand-compost along the MG1 and MG2 interfaces (Figure 2a) of the *modified Danish concept 1*, along the North-South direction. In this configuration, the thickness of the gas distribution layer along the North-South direction is not constant (Figure 2c), which results in different suction and water content values along the horizontal interfaces (MG1 and MG2), therefore in greater $\Delta\theta_w$ (or greater non-uniformity in terms of moisture). The thicker the gas distribution layer, the more it contributes to the drainage of accumulated moisture along the interface between the methane oxidation and gas distribution layers.

By Day 130, the θ_w values along the MG1 interface started to exceed the **conservative** $\theta_{w\text{-}occ}$ of the sand-compost. By Day 132, the MG1 interface was completely restricted (Figure 8b). By Day 126, the θ_w values in the sand-compost along the MG2 interface started to exceed the corresponding **conservative** $\theta_{w\text{-}occ}$, and by Day 139, the MG2 interface was completely restricted (Figure 8a).

Figure 9: Evolution of $LUGM_{MG1\text{-}pr}$ and $LUGM_{MG2\text{-}pr}$ in *modified Danish concept 1* (North-South direction)

The evolutions of $LUGM_{MG1\text{-}pr}$ and $LUGM_{MG2\text{-}pr}$ (defined in Figure 2c) in the *modified Danish concept 1* are shown in Figure 9 for the North-South direction It can be observed that $LUGM_{MG1\text{-}pr}$ remained equal to the total length of the interface, with the exception of a short

period of time (Day 139 to Day 142), when the upward flow of landfill gas across the interface was completely restricted. This restriction can be partly associated with the several rainy events that occurred previous to this period (see Figure 6b), which eventually led to moisture accumulation at the interface. Similar behaviour was observed for $LUGM_{MG2\text{-}pr}$. In both cases, the geometrical features of the biosystems (slope, thickness of layers, etc.) and characteristics of the materials composing them also play an important role and are at the core of the design process.

Considering the different shapes of the interfaces along the North-South and the West-East directions of the *modified Danish concept 1*, its hydraulic behavior is 3D. Therefore, the results obtained from 2D analyses in SEEP/W, i.e. Figure 7 to Figure 9, may change in a 3D analysis. For example, the rather unrestricted interface along the North-South direction (Figure 8) may help the interface along the West-East direction to possess greater values of $LUGM_{cg}$ than that associated with Figure 7b. On the other hand, the rather restricted interface along the North-South direction (Figure 8b) may result in obtaining $LUGM_{MG1\text{-}pr}$ and $LUGM_{MG2\text{-}pr}$ values lower than those obtained in Figure 9.

Figure 10: Evolution and distribution of (a) θ_w in the sand-compost along the MOL-GDL interface, and (b) $LUGM_{cg}$ - *modified Danish concept 2* (West-East direction)

As a prompt solution to increase $\Delta\theta_w$ along the jagged interfaces (West-East direction) of the *modified Danish concept 1*, the width of each segment was arbitrarily increased to 4 m, while the slope of the interface at each segment remained the same. This modification led to the creation of the *modified Danish concept 2*.

Figure 10 shows the evolution of $LUGM_{cg}$ and the distribution of θ_w for the *modified Danish concept 2*. As shown in Figure 10a, for the first time, on Day 132, θ_w values on the lower parts of each segment exceeded the **conservative** $\theta_{w\text{-}occ}$ for the sand-compost. The interface remained partially unrestricted until the end of the simulation period. The time associated with the partial restriction of the interface in the *modified Danish concept 2* (114 days) was longer than the time given by the *modified Danish concept 1* (47 days; Figure 8a). The maximum value of $\Delta\theta_w$ (5.1%) occurred on Day 198 where the interface was still partially unrestricted. The results in Figure 10 show that increasing the width of each segment resulted in an unblocked interface, albeit the short LUGM ($LUGM_{cg}$ in this case). In other words, fugitive landfill gas emissions reaching the base of the methane oxidation layer in a configuration, such as the *modified Danish concept 2* (and with the materials and width of segments adopted), would have to seep through a narrow channel within this layer.

Figure 11: Evolution of $LUGM_{MG2\text{-}pr}$ in *modified Danish concept 2* (North-South direction)

The evolution of $LUGM_{MG2\text{-}pr}$, i.e. LUGM along the interface in the North-South direction, for the *modified Danish concept 2* is presented in Figure 11. The value of $LUGM_{MG2\text{-}pr}$ remained close to the entire length of the North-South interface. In other words, landfill gas migration was almost completely unrestricted. The evolution of $LUGM_{MG1\text{-}pr}$ (along the MG1 interface) during the simulation is not presented, since it followed the same trend as the evolution of $LUGM_{MG1\text{-}pr}$ for the *modified Danish concept 1* (presented in Figure 9).

3.2. Alternative Danish concept

506 In the preceding section, it was shown that increasing the width of each segment could
507 increase the magnitude of $LUGM_{cg}$, i.e. the width of the channel through which landfill gas
508 reaches the methane oxidation layer. However, as shown in Figure 10b, the width of the
509 channel may be quite short and potentially lead to hotspot creation.

510 According to the results presented by Ahoughalandari and Cabral (2017), greater values of the
511 van Genuchten parameter *n* and greater saturated hydraulic conductivities of the MOL
512 material lead to greater $\Delta\theta_w$ along the sloping interface. The fine sand used in the
513 multi-material methane oxidation layer of the *alternative Danish concept* possesses a greater
514 saturated hydraulic conductivity and greater *n* than the values associated with the sand-
515 compost mixture of the *modified Danish concepts*. In addition, the slope of the k_a-function of
516 the fine sand when $\theta_a > \theta_{a\text{-}occ}$ (Figure 5a) is greater than the slope of the k_a function of the
517 sand-compost mixture when $\theta_a >$ **conservative** $\theta_{a\text{-}occ}$ (Figure 5b). Accordingly, when dry
518 density is maintained constant, the variation of gas intrinsic permeability with moisture in the
519 fine sand is greater than that associated with the sand-compost (i.e. MOL material of the
520 *modified Danish concepts*).

521 Therefore, using the selected fine sand as MOL material leads to greater drainage capacity,
522 therefore less moisture accumulation and greater differences in landfill gas fluxes at the base
523 of the methane oxidation layer. Consequently, constructing a methane oxidation layer with
524 sand-compost overlying the fine sand could potentially be a convenient alternative to the
525 *modified Danish concepts* in providing longer LUGMs. It is noteworthy to recall that very
526 high methane oxidation capacities have been found with this combination of materials
527 (denominated herein *alternative Danish concept*) in different situations (Ndanga et al. 2015).

528

529 Figure 12: Distribution and evolution of (a) θ_w in sand-compost, and (b) θ_w in fine sand -
530 *alternative Danish concept*, along the interface between sand-compost and fine sand layers
531 (West-East direction)

532

533 Figure 12 presents the distribution and evolution of θ_w in the sand-compost and fine sand
534 along the interface between the two materials, which may compose the upper-most capillary
535 barrier of the *alternative Danish concept* due to the contrast in their hydraulic properties. As
536 shown in Figure 12a, the θ_w values never attained the **conservative** $\theta_{w\text{-}occ}$ value for
537 sand-compost (50.5%). The θ_w values in the fine sand along the interface between the fine
538 sand and sand-compost layers were always lower than the $\theta_{w\text{-}occ}$ value for the fine sand, i.e.
539 30% (Figure 12b). Therefore, the interface between the sand-compost layer and the fine sand
540 layer was always unrestricted for upward flow of landfill gas. Indeed, during the period of
541 simulation, the $LUGM_{cf}$ was equal to the total length of the PMOB.

542

543 Figure 13: Evolution and distribution of (a) θ_w in the fine sand along the interface between the
544 fine sand layer and gas distribution layer, and (b) $LUGM_{fg}$ - *alternative Danish concept*
545 (West-East direction)

546

547 Figure 13 presents the evolution and distribution of θ_w in the fine sand along the interface
548 between the fine sand layer and the gas distribution layer, and the evolution of $LUGM_{fg}$ in the
549 second capillary barrier of the *alternative Danish concept*. Figure 13a shows that on Day 74
550 the θ_w values in the fine sand started to exceed the $\theta_{w\text{-}occ}$ but restriction to gas migration was
551 limited to a region whose length was less than 50% of the total length of the jagged segment.

552

553 Figure 14: Evolution and distribution of θ_w in the (a) sand-compost, and (b) fine sand along
554 the interface between the sand-compost and fine sand layers - *alternative Danish concept*, and
555 considering the interface between the fine sand layer and gas distribution layer in position
556 FG1, i.e. at the crest of the jagged interface (North-South direction)

557

558 Figure 14 presents the evolution of θ_w in the sand-compost and fine sand, along their North to
559 South interface within the *alternative Danish concept*. This simulation considered the
560 interface between the fine sand and gravel located at the crest of the segment, i.e. FG1 (Figure
561 4a). It can be observed that the θ_w values in the sand-compost and fine sand never attained the
562 design occlusion values, i.e. their **conservative** $\theta_{w\text{-}occ}$ (50.5% and 30% respectively).
563 Therefore, the $LUGM_{cf\text{-}pr}$ was always equal to the total length of the interface, meaning that
564 upward landfill gas flow was always unrestricted.

565

566 Figure 15: Evolution and distribution of θ_w in fine sand along the FG1 interface - *alternative*
567 *Danish concept* (North-South direction)

568

569 Figure 15 presents the evolution and distribution of θ_w in the fine sand, along the FG1 (fine
570 sand-gravel) interface in the North-South direction of the *alternative Danish concept*.
571 Performing a set of trial and error simulations, the slope of the interface was selected so that
572 θ_w values in the fine sand remained permanently lower than the $\theta_{w\text{-}occ}$, i.e. the landfill gas
573 intercepted by the gas distribution layer could flow unrestrictedly upward.

For the simulation considering the fine sand-gravel interface located along the FG2 interface (Figure 4a), the θ_w values in the sand-compost and fine sand along their interface, and in the fine sand along the FG2 interface were quite similar to the results presented in Figure 14 and Figure 15. Indeed, the θ_w values never attained the **conservative** $\theta_{w\text{-}occ}$ in the sand-compost and the $\theta_{w\text{-}occ}$ in the fine sand, meaning that, during the simulation, these interfaces were never restricted for upward flow of landfill gas.

The results presented in Figure 13 to Figure 15 show that $LUGM_{cf\text{-}pr}$, $LUGM_{FG1\text{-}pr}$ and $LUGM_{FG2\text{-}pr}$ (defined in Figure 4) were always equal to the total length of the corresponding interfaces, meaning that none of the interfaces along the North-South direction of the *alternative Danish concept* restricted upward flow of landfill gas. Using convenient MOL materials that are consistent with the requirements of the geometric features suggested in the *alternative Danish concept*, it is expected that greater LUGM values would be found, which means that unrestricted passages for upward flow of landfill gas would be ensured along the width and length of the PMOB. The simulations also showed that suction values would be sufficiently high to prevent water percolation into the gas distribution layer (data not presented).

4. Conclusions

The results of the transient-state numerical simulations to assess the behavior of two configurations for passive methane oxidation biosystems (PMOB) showed that after a certain period of time upward flow of landfill gas in one of the configurations tested became completely restricted. This restriction can be partly associated with the geometrical features of the configurations, the hydraulic characteristics of the unsaturated soil (i.e. water retention curve and hydraulic conductivity function) of the materials composing them, and with rainy

events that resulted in moisture accumulation at the interface between the gas distribution and methane oxidation layers. Such accumulations could potentially lead to the development of hotspots, i.e. regions on the surface where landfill gas concentrations are high. We therefore conclude that this configuration may in practice have limitations in terms of uniformity of landfill gas distribution and restriction to upward flow of landfill gas, depending on the materials used and geometry adopted.

In configurations with a jagged interface (a concept recently proposed by Danish colleagues), one has to perform a balancing act between keeping a wide enough unrestricted channel for landfill gas flow around the crest of each segment, and a large enough difference in moisture content values between the top and the bottom. This balance was conveniently achieved by an appropriate choice of geometrical features and materials whose greater drainage capacity resulted in less moisture accumulation and greater differences in landfill gas fluxes at the base of the methane oxidation layer. These characteristics dictate the magnitude of the length of unrestricted gas migration (LUGM), i.e. the design criterion. The paper stresses the importance of following a formal design process that includes a clear design criterion (or criteria) and parameter(s) that account for various phenomena influencing passive methane oxidation, such as the capillary barrier effect.

Acknowledgements

This study received financial support from the Natural Science and Engineering Research Council of Canada (NSERC) and Waste Management (WM Quebec Inc.), under the collaborative research and development grant # CRD 379885-08, and from Discovery Grant #170226. The Authors would like to acknowledge the invaluable help of Jean-Guy Lemelin, technician, and Behna Ahoughalandari for her help with graphic design.

References

Adu-Wusu, C., and Yanful, E.K. 2006. Performance of Engineered Test Covers on Acid-Generating Waste Rock at Whistle Mine, Ontario. Canadian Geotechnical Journal **43**(1): 1-18.

Ahoughalandari, B. 2016. Design of Passive Methane Oxidation Biosystems Considering their Response to the Presence of Capillary Barrier Effect. *In* Department of Civil Engineering. Université de Sherbrooke, Sherbrooke, Quebec, Canada. p. 142.

Ahoughalandari, B., and Cabral, A.R. 2017. Influence of capillary barrier effect on biogas distribution at the base of passive methane oxidation biosystems: Parametric study. Waste Management **63**: 172-187. doi: 10.1016/j.wasman.2016.11.026.

ASTM-D2434-68. 2006. Standard Test Method for Permeability of Granular Soils (Constant Head). ASTM International, West Conshohocken, PA.

ASTM-D6539-13. 2006. Standard Test Method for Measurement of the Permeability of Unsaturated Porous Materials by Flowing Air. ASTM International, West Conshohocken, PA.

Bussière, B., Aubertin, M., and Chapuis, R.P. 2003. The Behavior of Inclined Covers Used as Oxygen Barriers. Canadian Geotechnical Journal **40**: 512-535.

Cabral, A., Racine, I., Burnotte, F., and Lefebvre, G. 2000. Diffusion of oxygen through a pulp and paper residue barrier. Canadian Geotechnical Journal **37**(1): 201-217.

Cabral, A.R., Létourneau, M., Yanful, E., Song, Q., McCartney, J.S., and Parks, J. 2010. Geotechnical Issues in the Design and Construction of PMOBs. *In* UNSAT 2010, Barcelona. pp. 1361-1367.

644 Capanema, M.A., and Cabral, A.R. 2012. Evaluating Methane Oxidation Efficiencies in
645 Experimental Landfill Biocovers by Mass Balance and Carbon Stable Isotopes. Water Air
646 Soil Pollut **223**(9): 5623-5635.

647 Cassini, F., Scheutz, C., Skov, B.H., Mou, Z., and Kjeldsen, P. 2017. Mitigation Of Methane
648 Emissions In A Pilot-Scale Biocover System At The Av Miljo Landfill, Denmark: 1. System
649 Design And Gas Distribution. Waste Management **27**: (in press). doi:
650 10.1016/j.wasman.2017.01.013.

651 Chanton, J., Abichou, T., Langford, C., Hater, G., Green, R., Goldsmith, D., and Swan, N.
652 2011. Landfill Methane Oxidation Across Climate Types in the U.S. Environ. Sci. Technol.
653 **45**: 313-319.

654 Chapuis, R.P. 2004. Predicting the Saturated Hydraulic Conductivity of Sand and Gravel
655 Using Effective Diameter and Void Ratio. Can. Geotech. J. **41**: 787-795.

656 Fredlund, D.G., Rahardjo, H., and Fredlund, M.D. 2012. Unsaturated Soil Mechanics in
657 Engineering Practice. John Wiley & Sons, Inc., Hoboken, NJ, USA. pp. 9.

658 Fredlund, M.D., Wilson, G.W., and Fredlund, D.G. 2002. Use of the Grain-Size Distribution
659 for Estimation of the Soil-Water Characteristic Curve. Canadian Geotechnical Journal **39**:
660 1103-1117.

661 Geck, C., Gebert, J., Scharff, H., Streese-Kleeberg, J., and Pfeiffer, E.-M. 2012.
662 Heterogeneous Gas Distribution within a Biocover Designed for Methane Oxidation *In* 7th
663 Intercontinental Landfill Research Symposium (ICLRS). Poster presentation, Luleä, Sweden.

664 Geck, C., Scharff, H., Pfeiffer, E.-M., and Gebert, J. 2016. Validation of a Simple Model to
665 Predict the Performance of Methane Oxidation Systems, Using Field Data from a Large Scale
666 Biocover Test Field. Waste Management **56**: 280-289.

667 GEO-SLOPE. 2010. SEEP/W 2007 User's Manual. *Edited by* G.-S.I. Ltd.

668 He, R., Wang, J., Xia, F., Mao, L., and Shen, D. 2012. Evaluation of Methane Oxidation
669 Activity in Waste Biocover Soil During Landfill Stabilization. Chemosphere **89**: 672-679.

670 Huber-Humer, M., Gebert, J., and Hilger, H. 2008. Biotic Systems to Mitigate Landfill
671 Methane Emissions. Waste Management & Research **26**(1): 33-46.

672 Jucá, J., and Maciel, F. 2006. Gas Permeability of a Compacted Soil Used in a Landfill Cover
673 Layer. *In* Fourth International Conference on Unsaturated Soils. *Edited by* G.A. Miller and
674 C.E. Zapata and S.L. Houston and D.G. Fredlund. American Society of Civil Engineers,
675 Carefree, Arizona, United States. pp. 1535-1546.

676 Langfelder, L.J., Chen, C.F., and Justice, J.A. 1968. Air Permeability of Compacted Cohesive
677 Soils. Journal of the Soil Mechanics and Foundations Division **94**(4): 981-1002.

678 Leroueil, S., and Hight, D.W. 2013. Compacted Soils: From Physics to Hydraulic and
679 Mechanical Behaviour. *In* First Pan-American Conference on Unsaturated Soils. *Edited by*
680 C.M. Bernardo Caicedo, Laureano Hoyos, Julio Esteban Colmenares, Ivan Rafael Berdugo,
681 Cartagena, Colombia. pp. 41-59.

682 Lu, N., and Likos, W.J. 2004. Unsaturated Soil Mechanics. John Wiley & Sons, Inc. pp. 556.

683 Marinho, F.A.M., Andrade, M.C.J., and Jucá, J.F.T. 2001. Air and Water Permeability of a
684 Compacted Soil Used in a Solid Waste Landfill in Recife, Brazil. *In* the Third BGA

685 Geoenvironmental Engineering Conference. Thomas Telford Publishing, Thomas Telford
686 Ltd., Edinburg, Scotland. pp. 437-442.

687 Mualem, Y. 1976. A New Model For Predicting the Hydraulic Conductivity of Unsaturated
688 Porous Media. Water Resources Research **12**: 513-522.

689 Ndanga, É.M., Bradley, R.L., and Cabral, A.R. 2015. Does Vegetation Affect the Methane
690 Oxidation Efficiency of Passive Biosystems? Waste Management **38**: 240-249.

691 Rachor, I., Gebert, J., Groengroeft, A., and Pfeiffer, E.M. 2013. Variability of methane
692 emissions from an old landfill over different time-scales. European Journal of Soil Science
693 **64**: 16-26. doi: doi: 10.1111/ejss.12004.

694 Röwer, I.U., Gebert, J., Streese-Kleeberg, J., Kleinschmidt, V., Melchior, S., Scharff, H., and
695 Pfeiffer, E.-M. 2012. Heterogeneous Emission from a Biocover Designed for Methane
696 Oxidation. *In* 7th Intercontinental Landfill Research Symposium (ICLRS). Poster presentation,
697 Luleä, Sweden.

698 Rower, I.U., Geck, C., Gebert, J., and Pfeiffer, E.-M. 2011. Spatial variability of soil gas
699 concentration and methane oxidation capacity in landfill covers. Waste Management **31**(5):
700 926-934. doi: 10.1016/j.wasman.2010.09.013.

701 Scheutz, C., Kjeldsen, P., Bogner, J.E., De Visscher, A., Gebert, J., Hilger, H.A., Huber-
702 Humer, M., and Spokas, K. 2009. Microbial Methane Oxidation Processes and Technologies
703 for Mitigation of Landfill Gas Emissions. Waste Management and Research **27**(5): 409-455.

704 Spokas, K.A., and Bogner, J.E. 2011. Limits and Dynamics of CH4 Oxidation on Landfill
705 Cover Soils. Waste Management **31**: 823-832.

706 Springer, D.S., Loaiciga, H.A., Cullen, S.J., and Everett, L.G. 1998. Air Permeability of
707 Porous Materials Under Controlled Laboratory Conditions. Groundwater **36**(4): 558-565. doi:
708 10.1111/j.1745-6584.1998.tb02829.x.

709 Tang, A.M., Cui, Y.-J., Richard, G., and Défossez, P. 2011. A Study on the Air Permeability
710 as Affected by Compression of Three French Soils. Geoderma **162**: 171-181.

711 Tétreault, P., Cabral, A.R., and Abdolahzadeh, A.M. 2013. Non-uniform distribution of
712 biogas under a biocover due to capillary barrier effect: case studies. *In* 66th Canadian
713 Geotechnical Conference - GeoMontreal 2013. *Edited by* C.G. Society. Canadian
714 Geotechnical Society, Montreal. p. Paper 184.

715 UMS. 2013. HYPROP-UMS User's Manual. *In* Art. no. HYPROP Version 02. UMS GmbH
716 München.

717 van Genuchten, M.T. 1980. A Closed-Form Equation for Predicting the Hydraulic
718 Conductivity of Unsaturated Soils. Soil Science Society of America Journal **44**: 892-898.

719 Yanful, E.K. 1993. Oxygen Diffusion through Soil Covers on Sulphidic Mine Tailings.
720 Journal of Geotechnical Engineering **119**(8): 1207-1228.

721

Table 1: Hydraulic properties of the materials used in numerical simulations

Parameters	*Modified Danish concepts*		*Alternative Danish concept*		
	sand-compost	gravel	sand-compost	fine sand	gravel
a (kPa)	2.8	0.5	2.8	-	0.5
n	1.28	2.4	1.28	-	2.4
θ_s (%V/V)	67	30	67	36.6	30
θ_r (%V/V)	0.1	0	0.1	5	0
k_{sat} (m/s)	9.0×10^{-6}	4.3×10^{-2}	9.0×10^{-6}	9.0×10^{-5}	4.3×10^{-2}

Figure 1

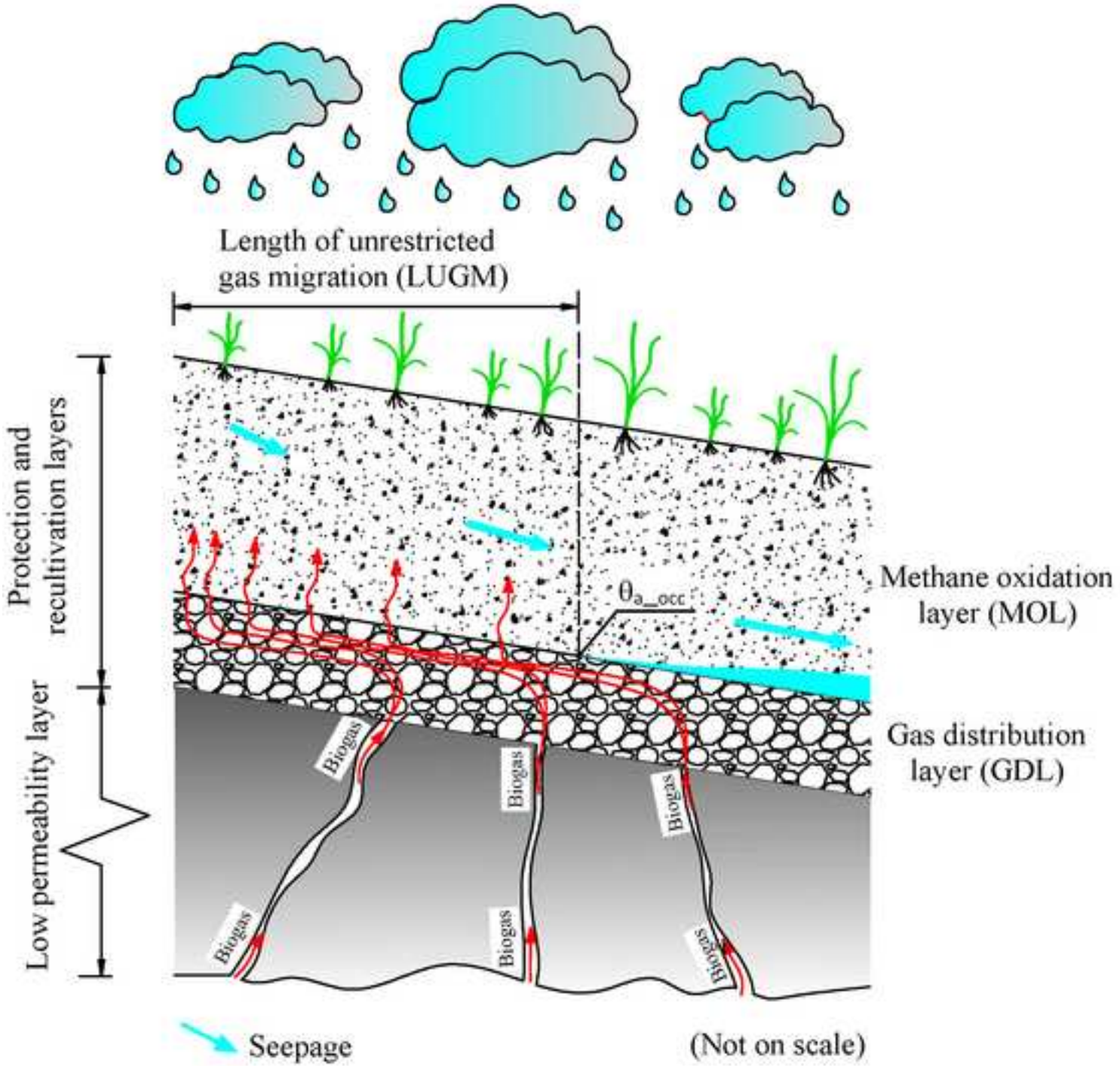
Length of unrestricted gas migration (LUGM)
Protection and recultivation layers
Low permeability layer
Methane oxidation layer (MOL)
Gas distribution layer (GDL)
θa_occ
Biogas
Biogas
Biogas
Biogas
Biogas
Biogas
Seepage
(Not on scale)

Figure 2a

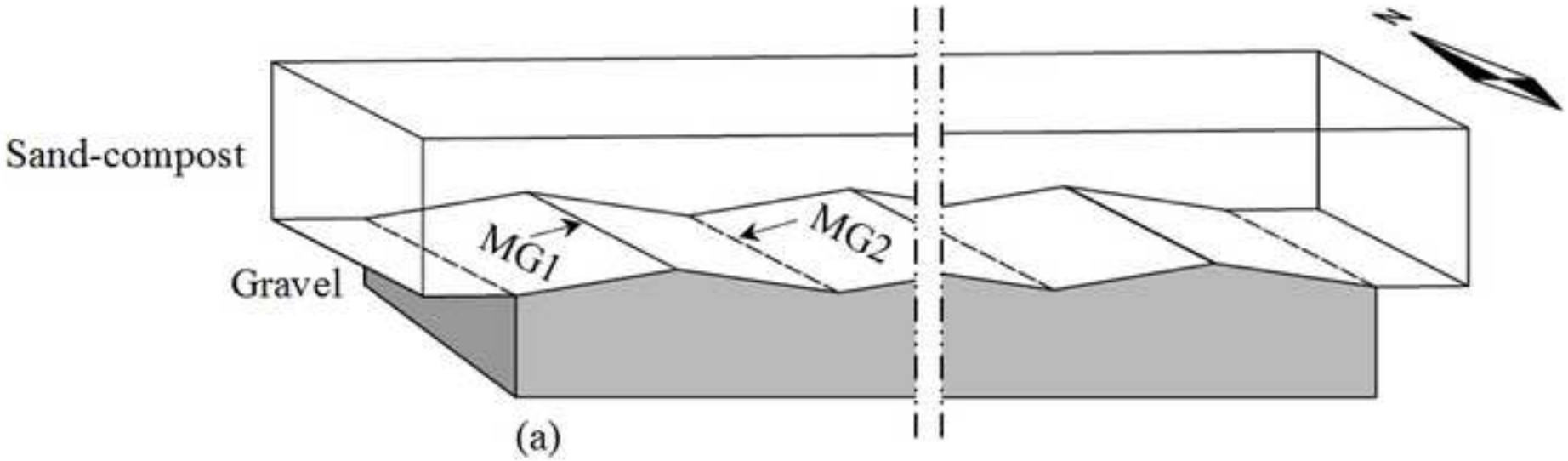

Figure 2b

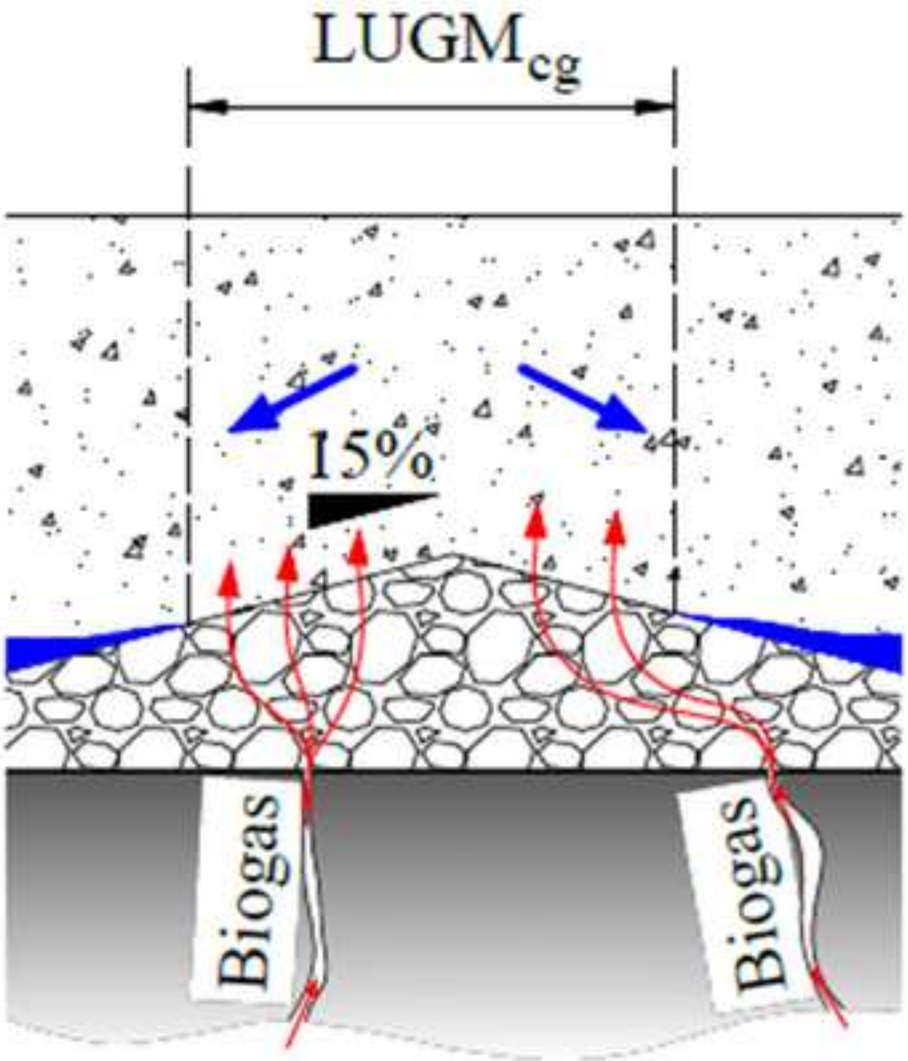

Sand-compost (80-90 cm)

Gravel (30-50 cm)

Waste

(b)

Figure 2c

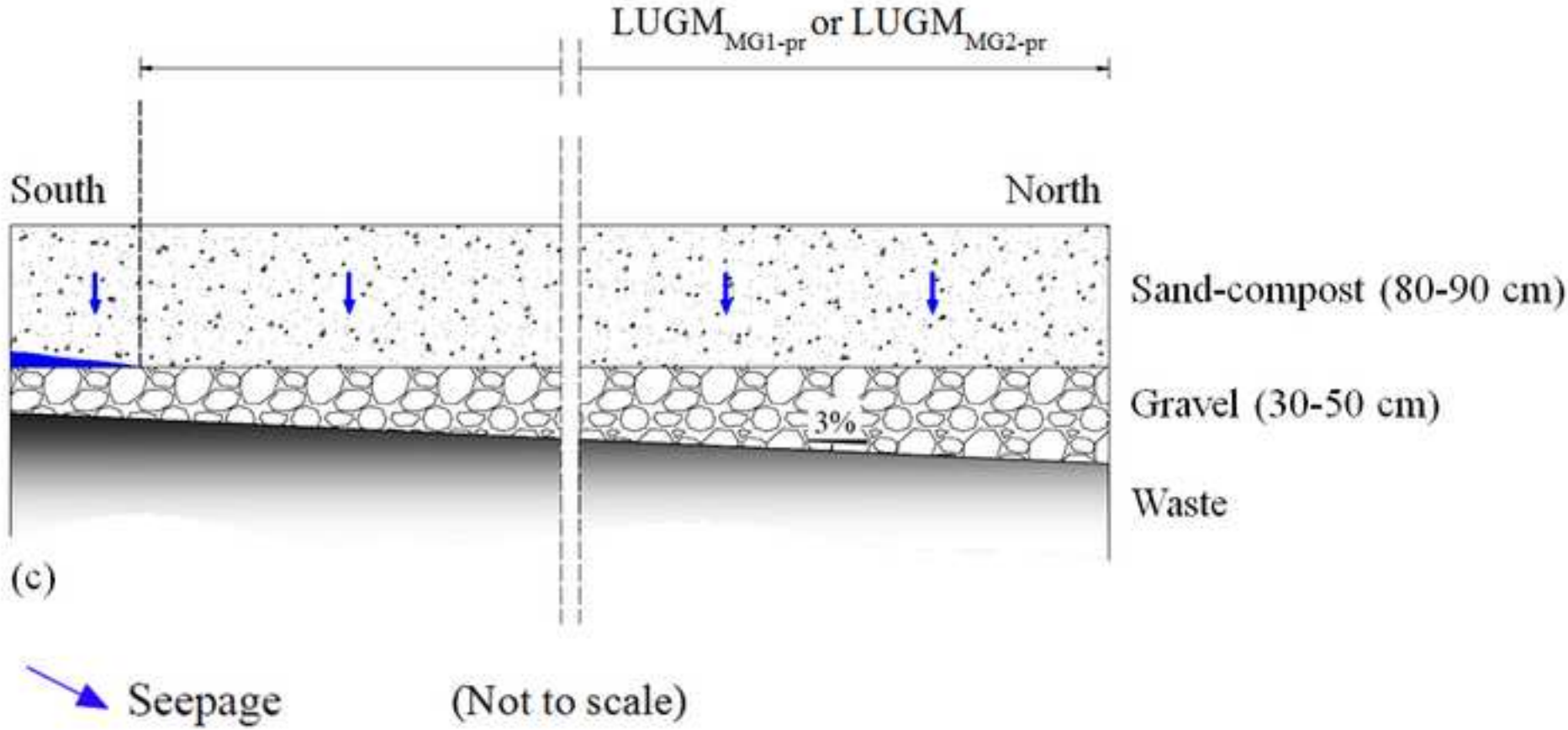
LUGM MG1-pr or LUGM MG2-pr
South
North
Sand-compost (80-90 cm)
Gravel (30-50 cm)
3%
Waste
(c)
Seepage
(Not to scale)

Figure 3a

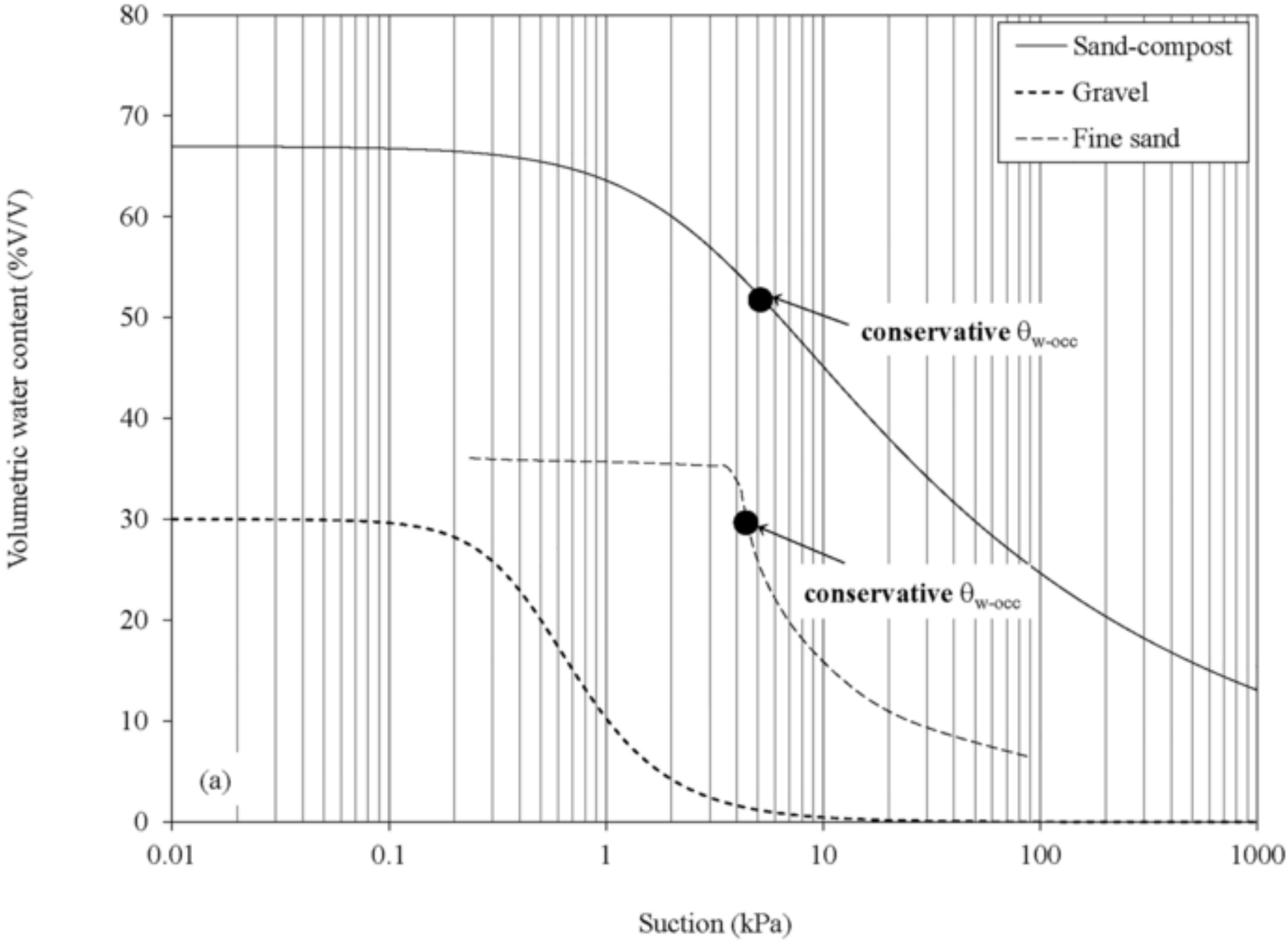
Sand-compost
Gravel
Fine sand
conservative $\theta_{w\text{-}occ}$
conservative $\theta_{w\text{-}occ}$
(a)
Volumetric water content (%V/V)
Suction (kPa)
0
10
20
30
40
50
60
70
80
0.01
0.1
1
10
100
1000

Figure 3b

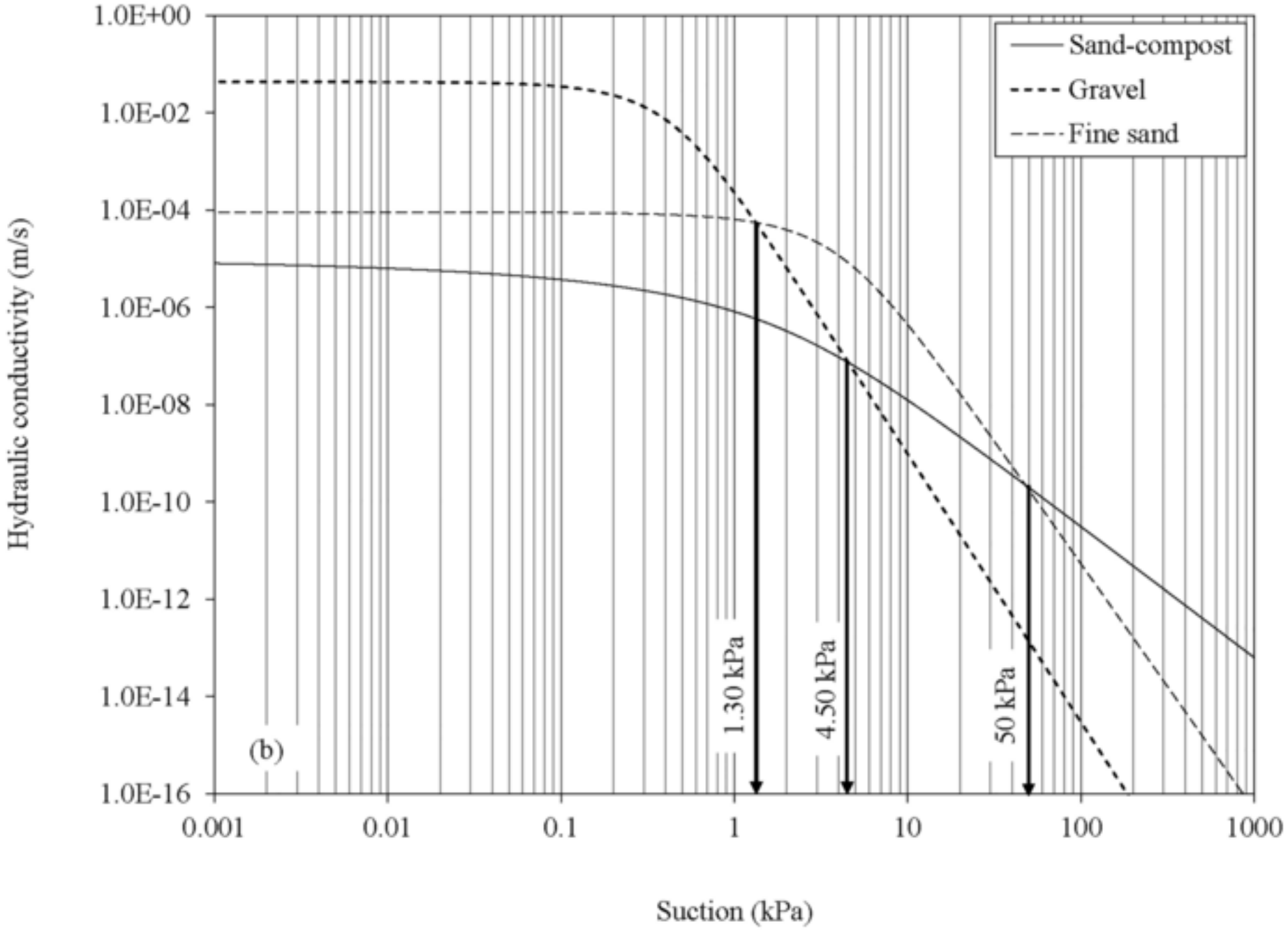
1.0E+00
1.0E-02
1.0E-04
1.0E-06
1.0E-08
1.0E-10
1.0E-12
1.0E-14
1.0E-16
Hydraulic conductivity (m/s)
0.001
0.01
0.1
1
10
100
1000
Suction (kPa)
Sand-compost
Gravel
Fine sand
1.30 kPa
4.50 kPa
50 kPa
(b)

Figure 4a

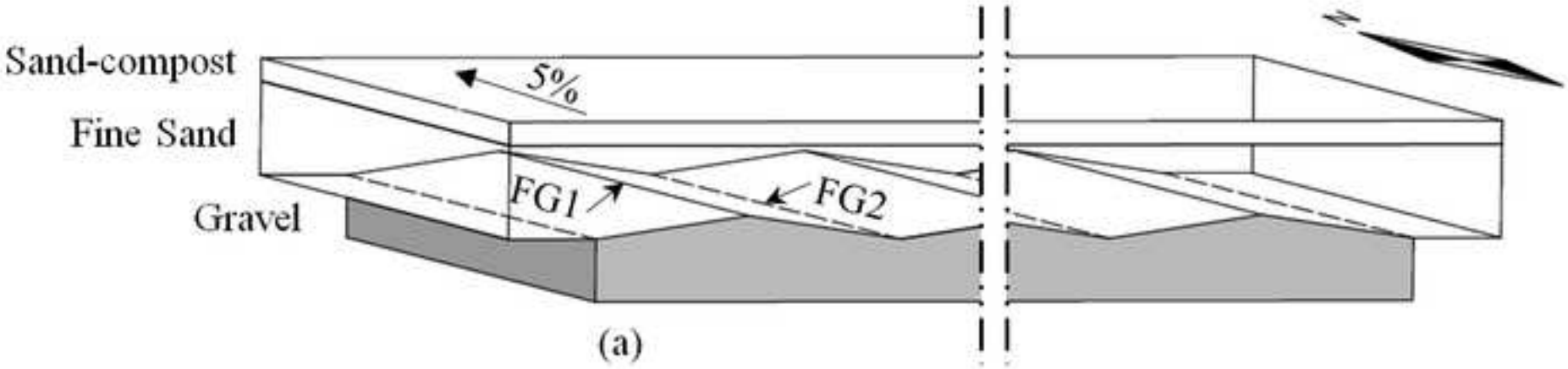

Figure 4b

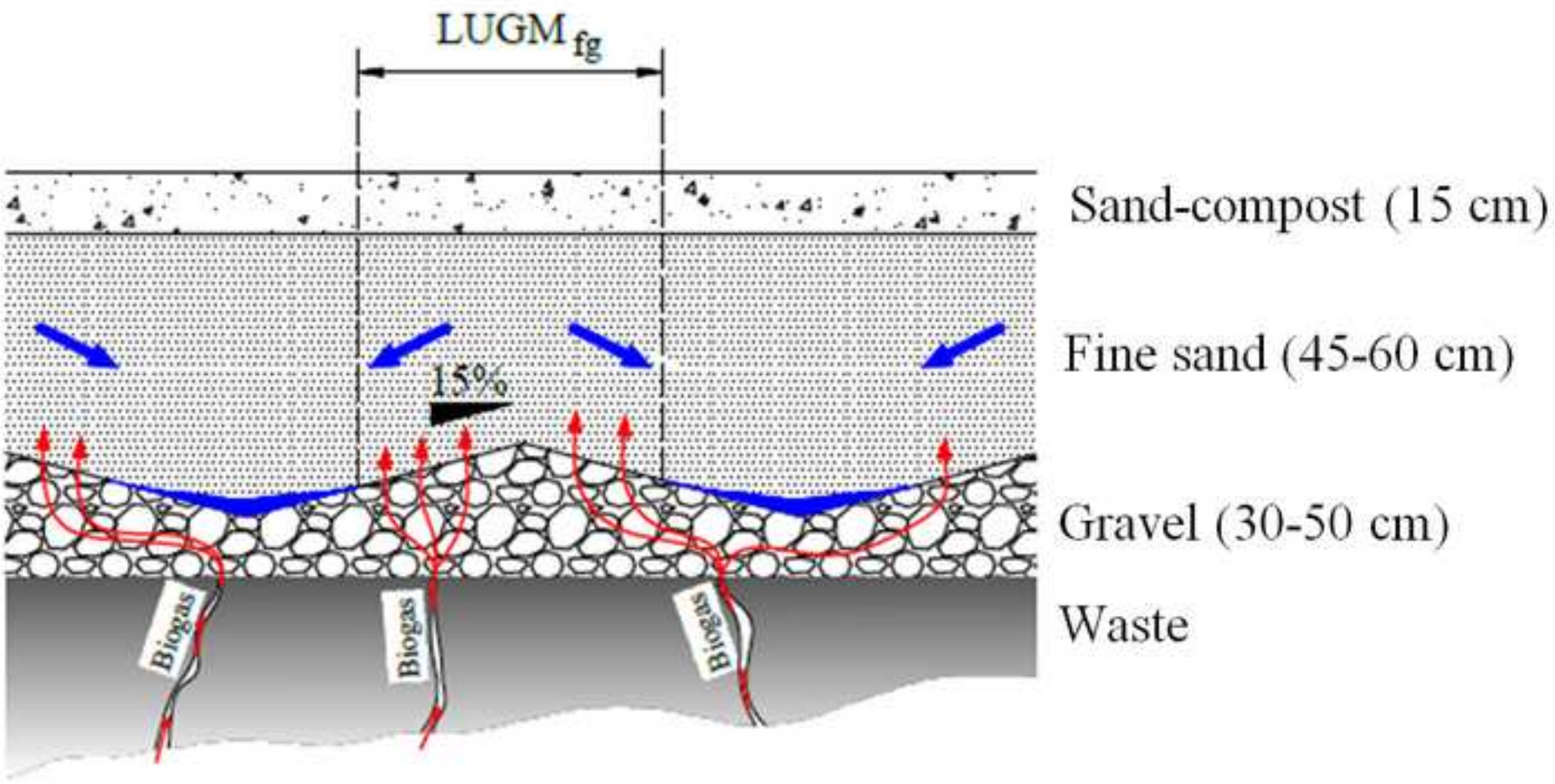
LUGM fg
Sand-compost (15 cm)
Fine sand (45-60 cm)
15%
Gravel (30-50 cm)
Waste
Biogas
Biogas
Biogas

(b)

Figure 4c

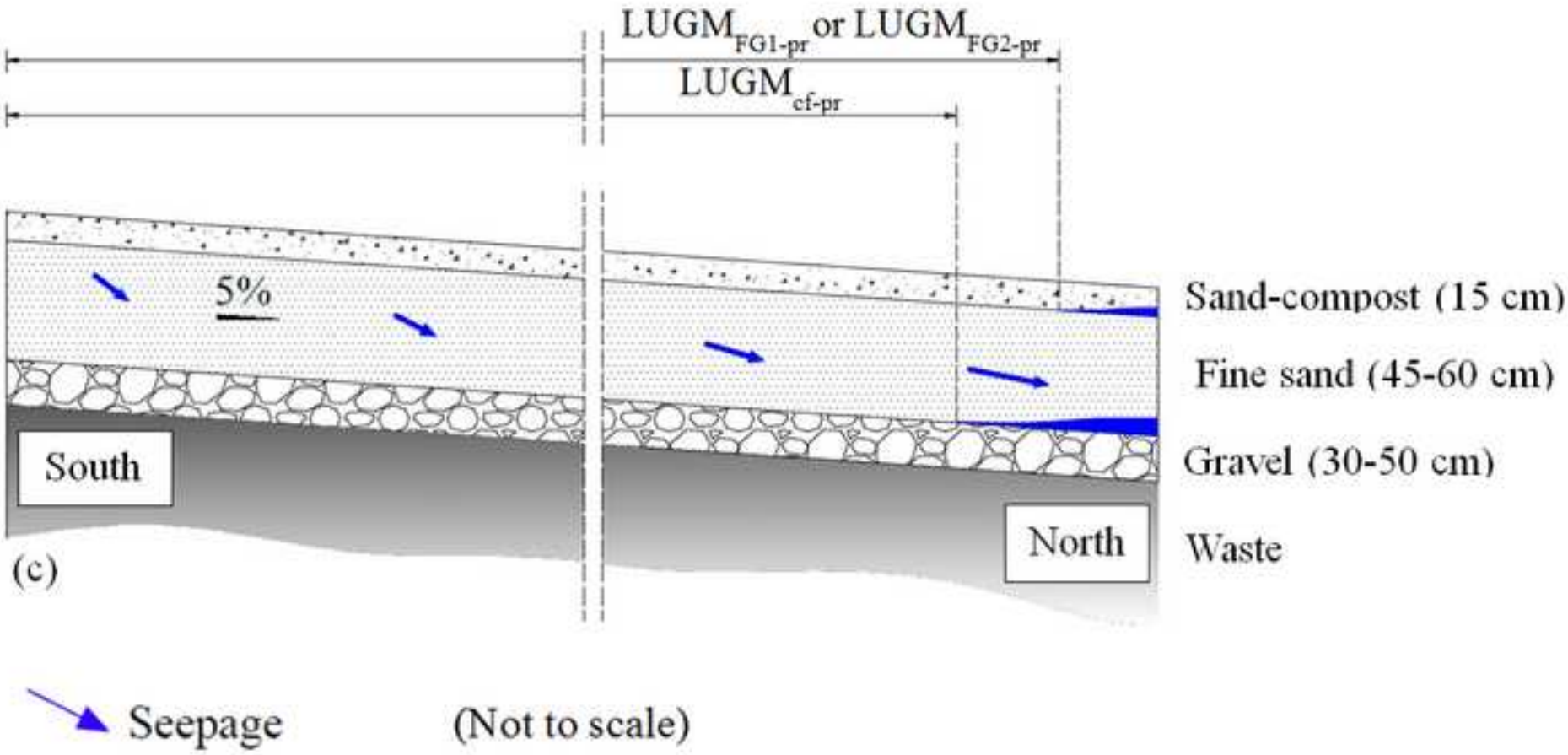
LUGM FG1-pr or LUGM FG2-pr
LUGM cf-pr
5%
South
North
(c)
Sand-compost (15 cm)
Fine sand (45-60 cm)
Gravel (30-50 cm)
Waste
Seepage
(Not to scale)

Figure 5a

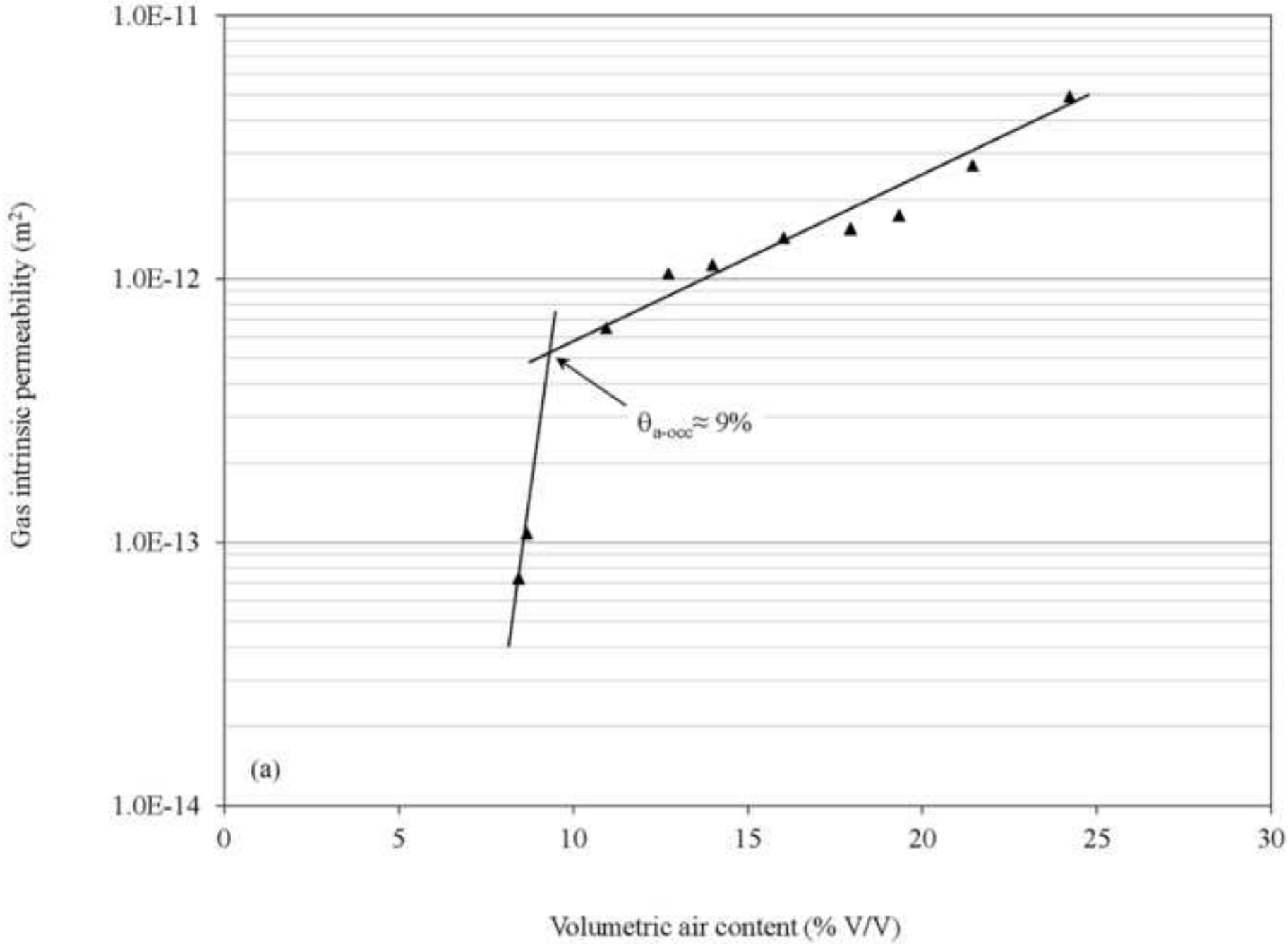
1.0E-11
1.0E-12
1.0E-13
1.0E-14
Gas intrinsic permeability (m²)
θa-occ≈ 9%
(a)
0
5
10
15
20
25
30
Volumetric air content (% V/V)

Figure 5b

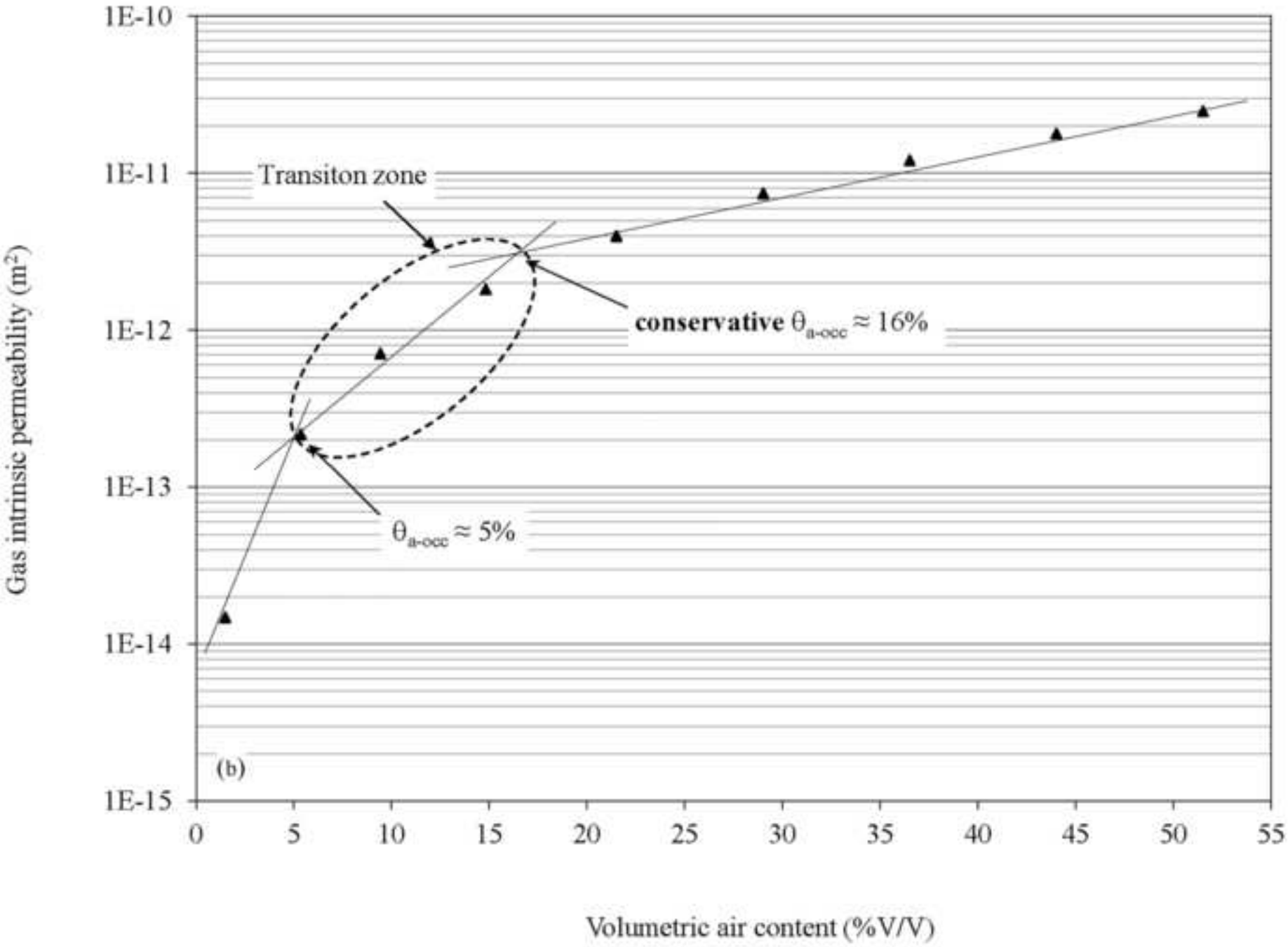
1E-10
1E-11
1E-12
1E-13
1E-14
1E-15
Gas intrinsic permeability (m²)
Transiton zone
conservative θa-occ ≈ 16%
θa-occ ≈ 5%
(b)
0
5
10
15
20
25
30
35
40
45
50
55
Volumetric air content (%V/V)

Figure 6

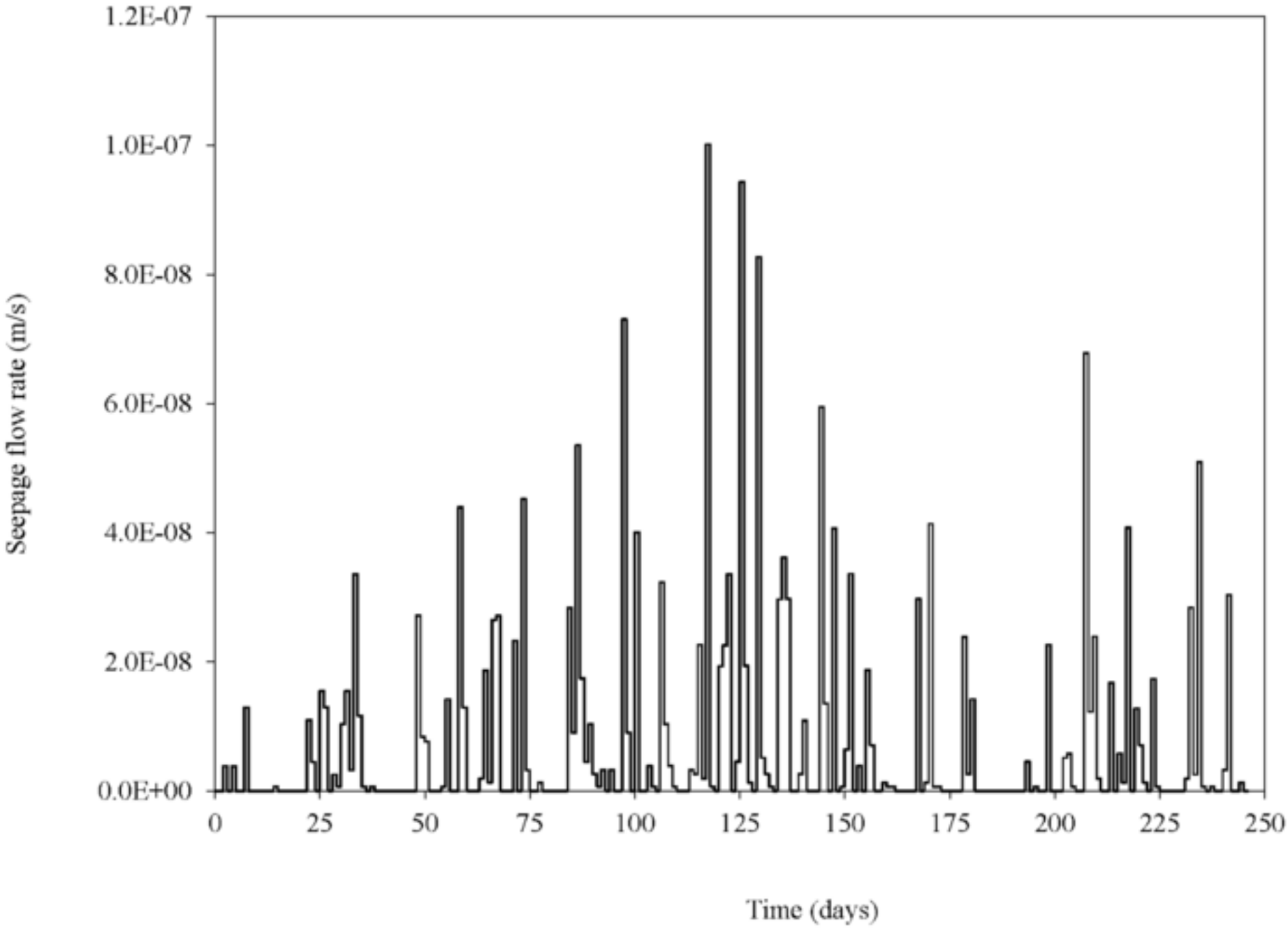
1.2E-07
1.0E-07
8.0E-08
6.0E-08
4.0E-08
2.0E-08
0.0E+00
Seepage flow rate (m/s)
0
25
50
75
100
125
150
175
200
225
250
Time (days)

Figure 7a

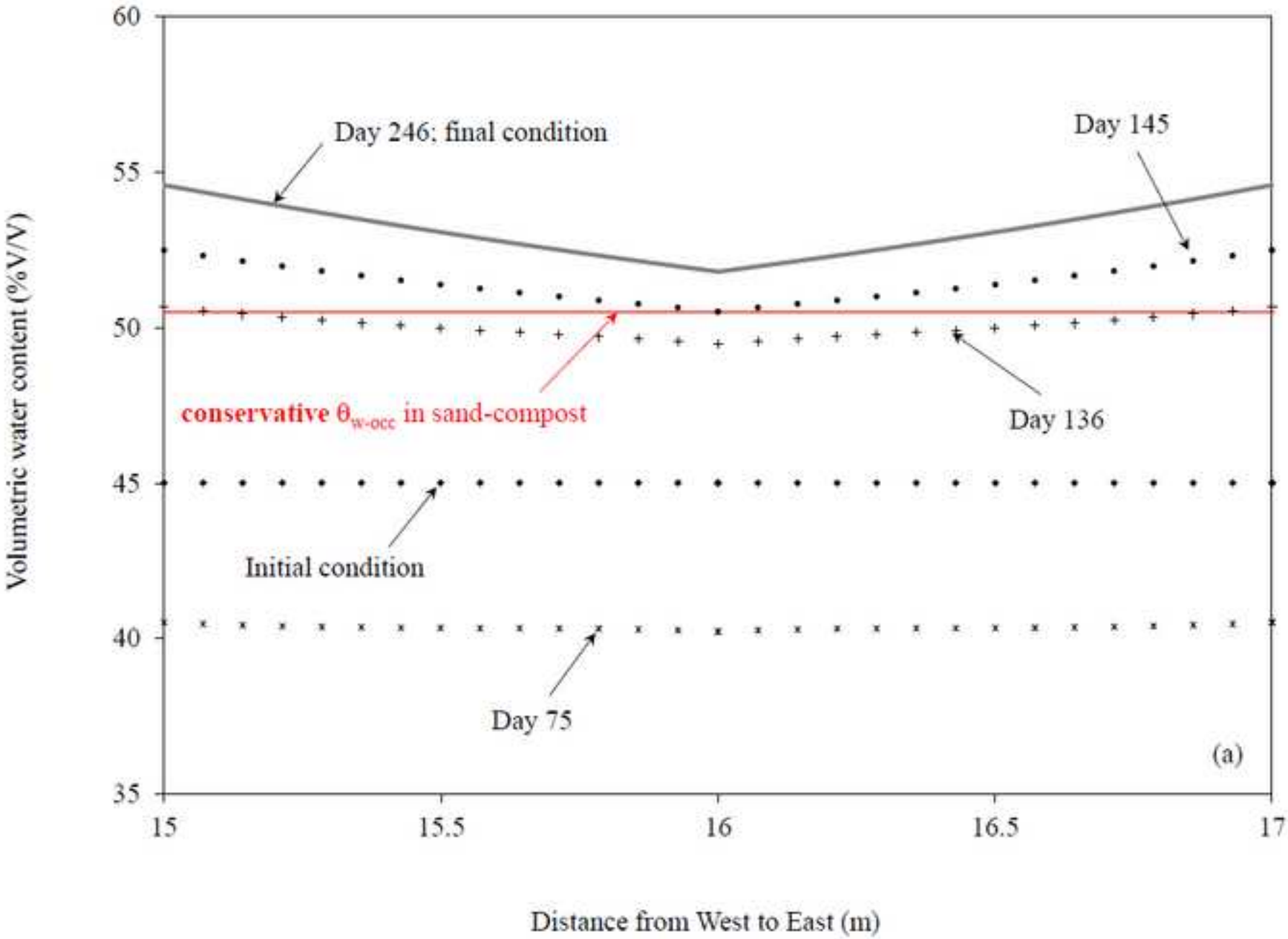
60
55
50
45
40
35
15
15.5
16
16.5
17
Volumetric water content (%V/V)
Distance from West to East (m)
Day 246: final condition
Day 145
conservative $\theta_{w\text{-}occ}$ in sand-compost
Day 136
Initial condition
Day 75
(a)

Figure 7b

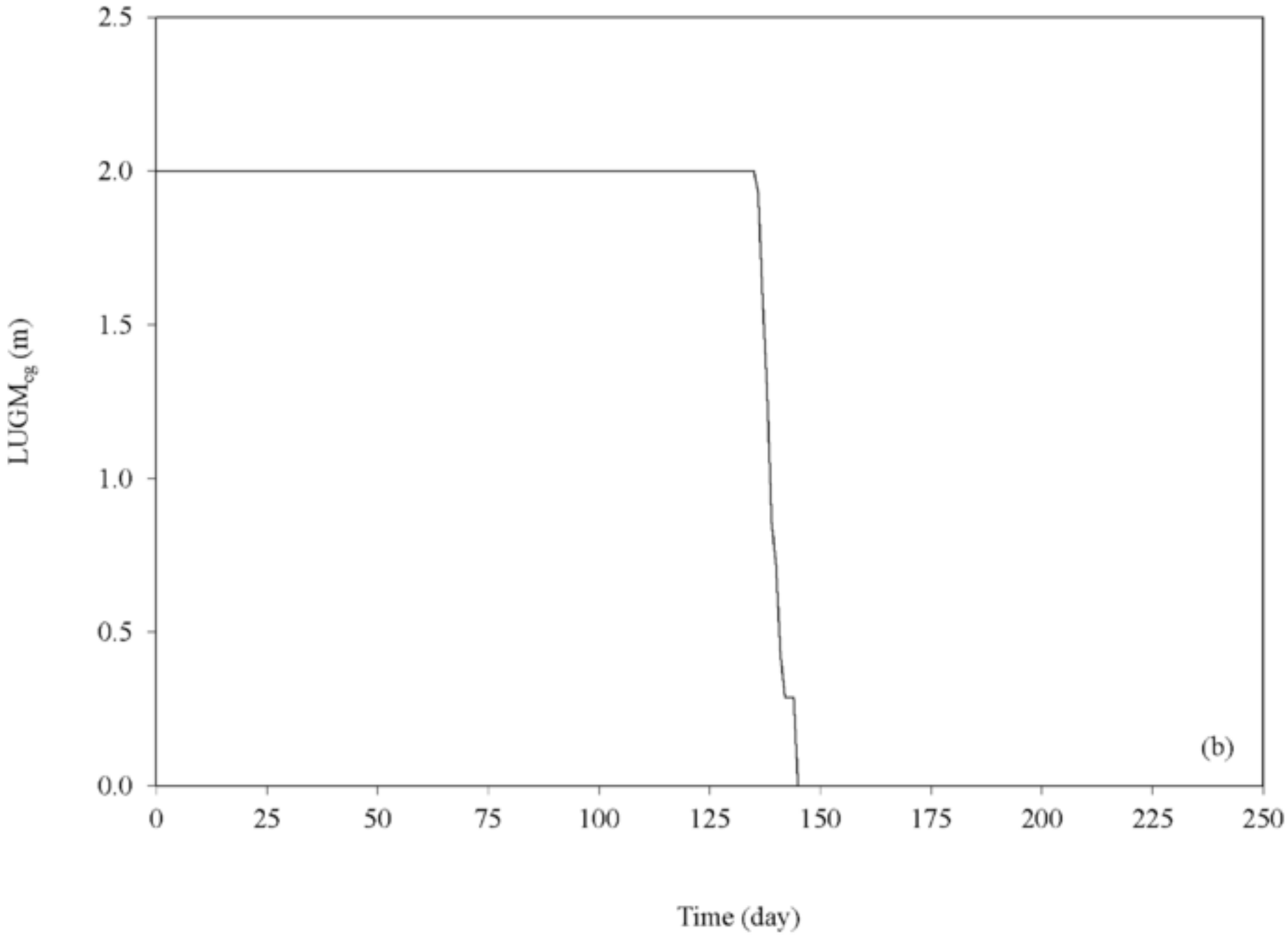
2.5
2.0
1.5
1.0
0.5
0.0
LUGM$_{cg}$ (m)
0
25
50
75
100
125
150
175
200
225
250
Time (day)
(b)

Figure 8a

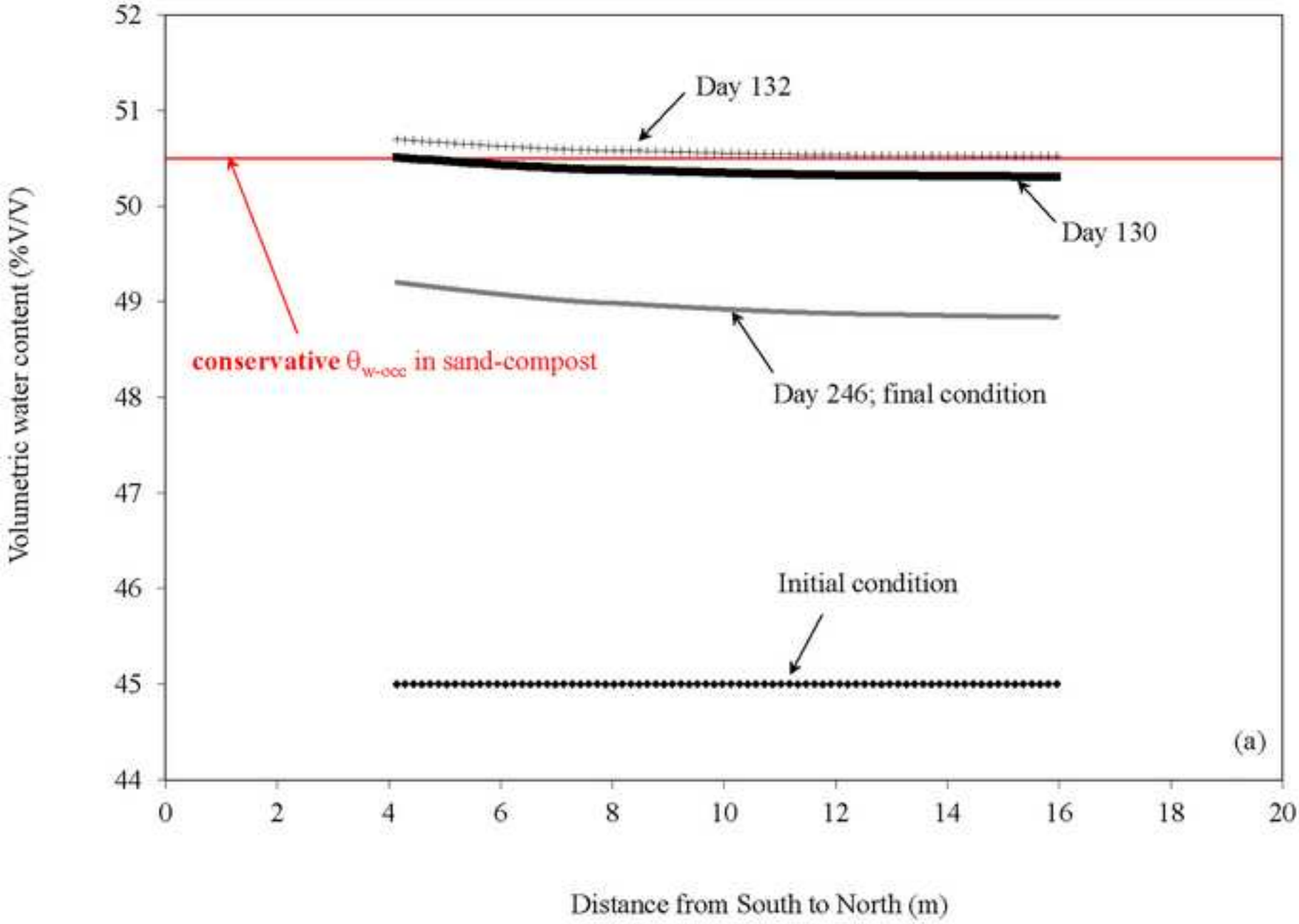
52
51
50
49
48
47
46
45
44
0
2
4
6
8
10
12
14
16
18
20
Volumetric water content (%V/V)
Distance from South to North (m)
Day 132
Day 130
Day 246; final condition
Initial condition
conservative θw-occ in sand-compost
(a)

Figure 8b

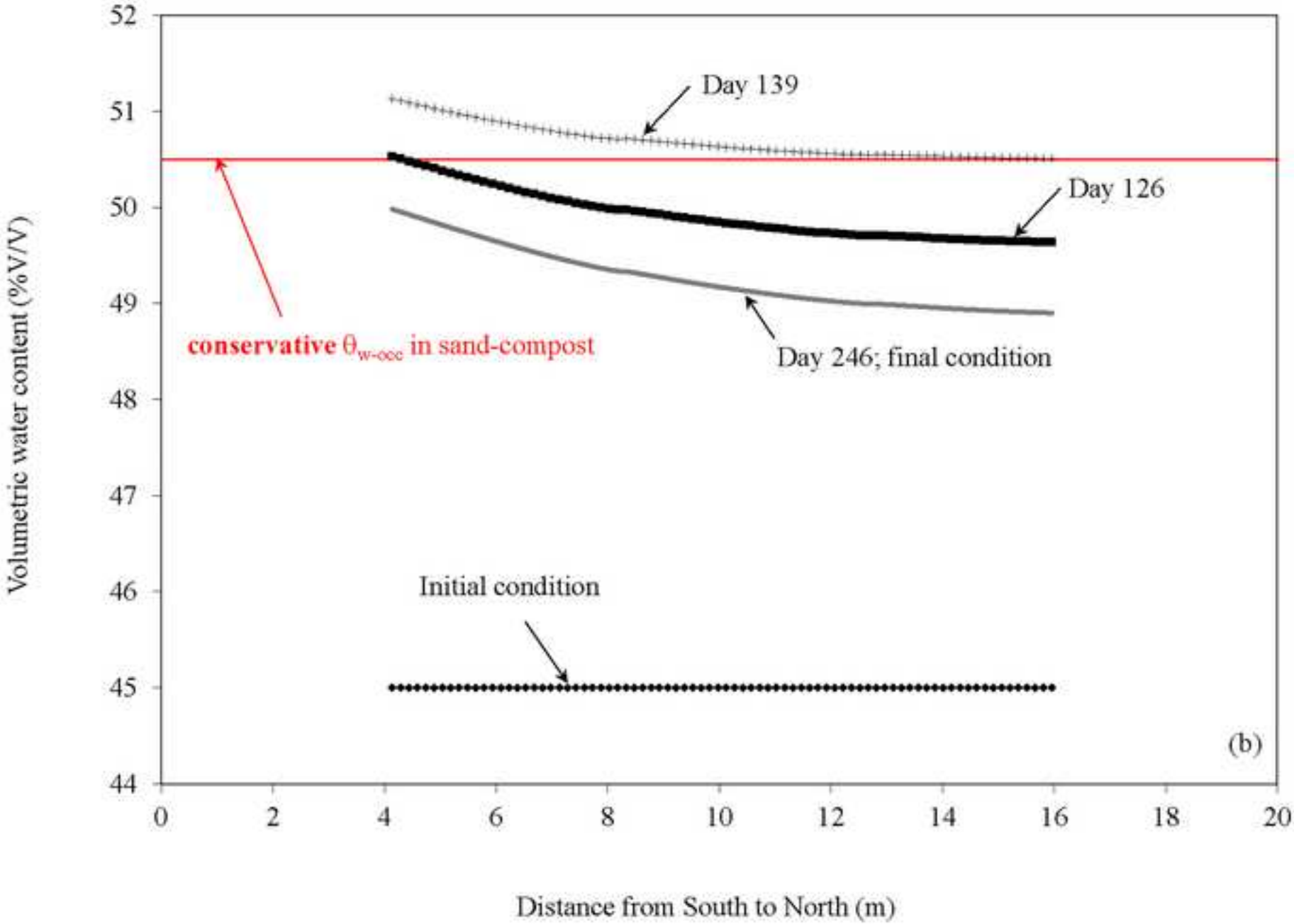
52
51
50
49
48
47
46
45
44
0
2
4
6
8
10
12
14
16
18
20
Volumetric water content (%V/V)
Distance from South to North (m)
Day 139
Day 126
Day 246; final condition
conservative θw-occ in sand-compost
Initial condition
(b)

Figure 9

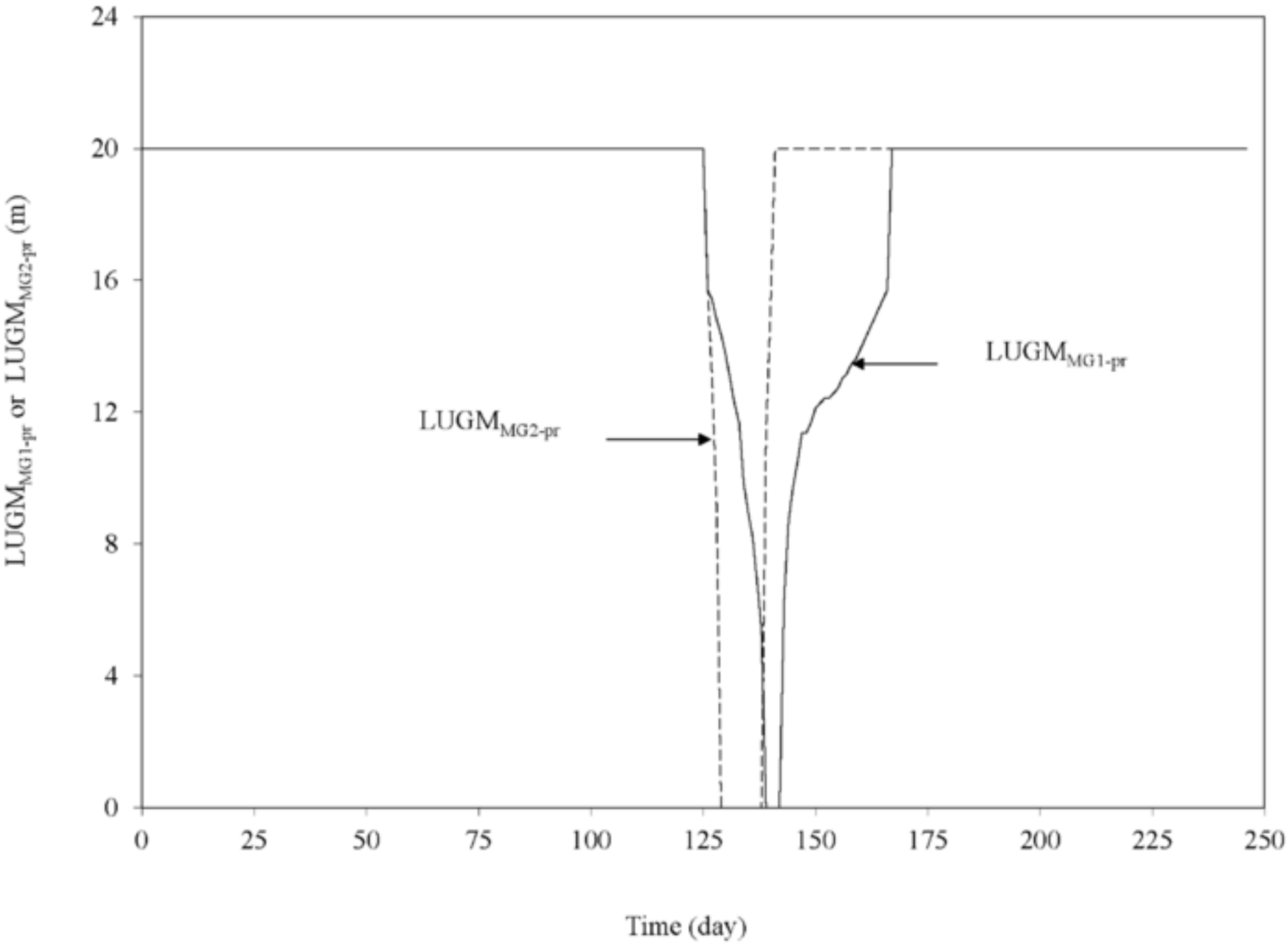
24
20
16
12
8
4
0
0
25
50
75
100
125
150
175
200
225
250
LUGM$_{MG1-pr}$ or LUGM$_{MG2-pr}$ (m)
Time (day)
LUGM$_{MG2-pr}$
LUGM$_{MG1-pr}$

Figure 10a

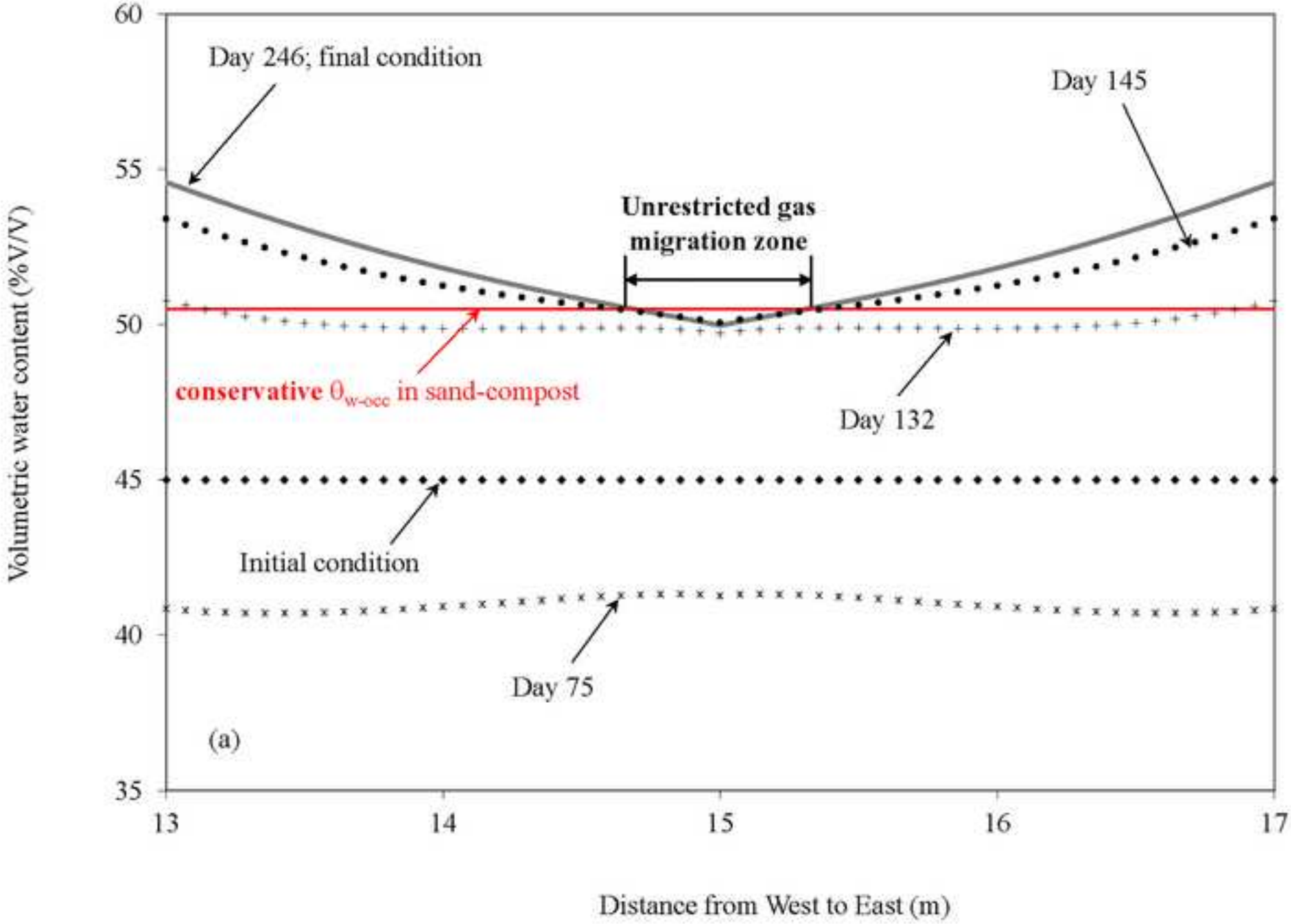
60
55
50
45
40
35
13
14
15
16
17
Volumetric water content (%V/V)
Distance from West to East (m)
Day 246; final condition
Day 145
Unrestricted gas migration zone
conservative $\theta_{w\text{-}occ}$ in sand-compost
Day 132
Initial condition
Day 75
(a)

Figure 10b

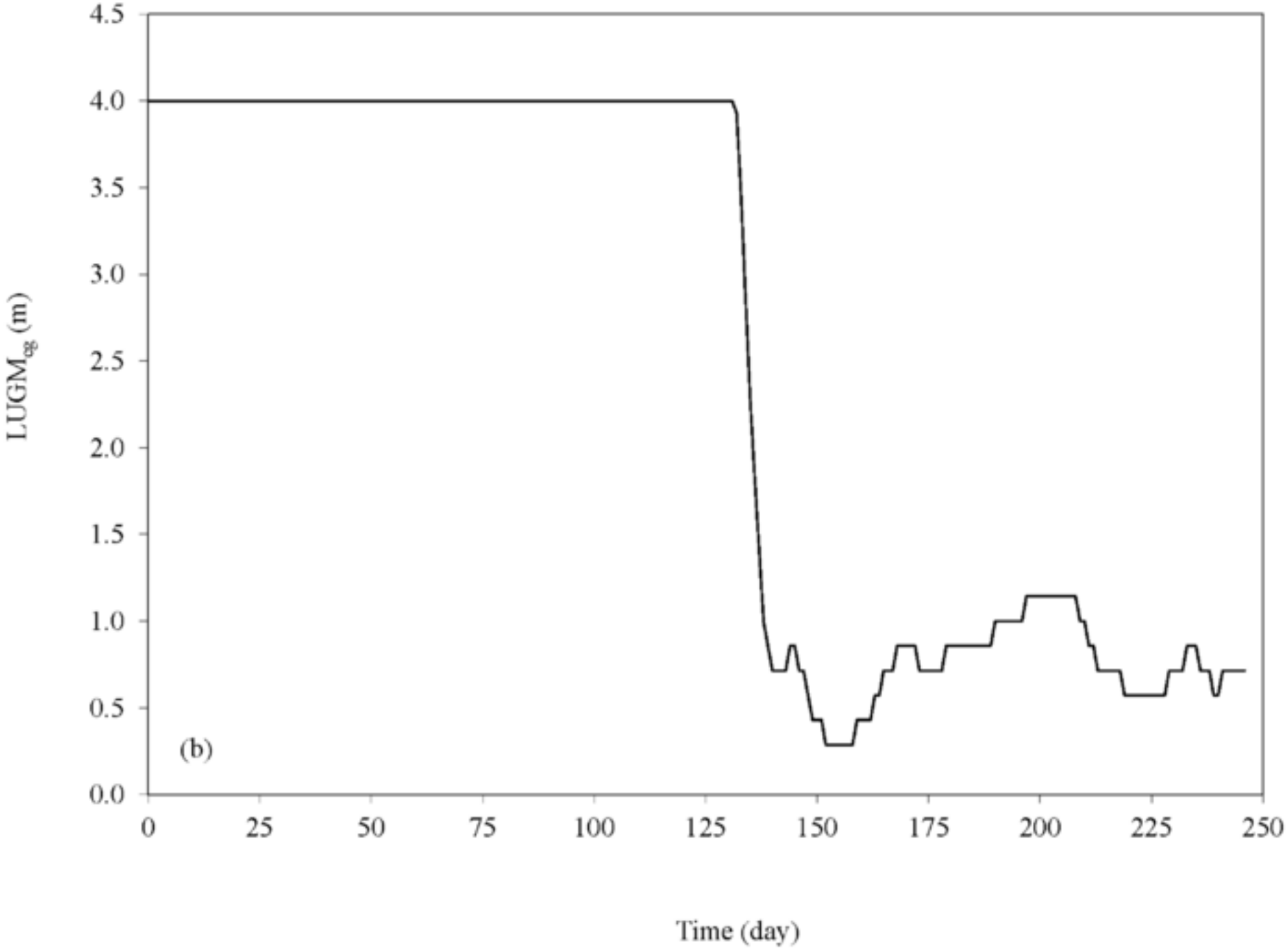
4.5
4.0
3.5
3.0
2.5
2.0
1.5
1.0
0.5
0.0
LUGM$_{og}$ (m)
(b)
0
25
50
75
100
125
150
175
200
225
250
Time (day)

Figure 11

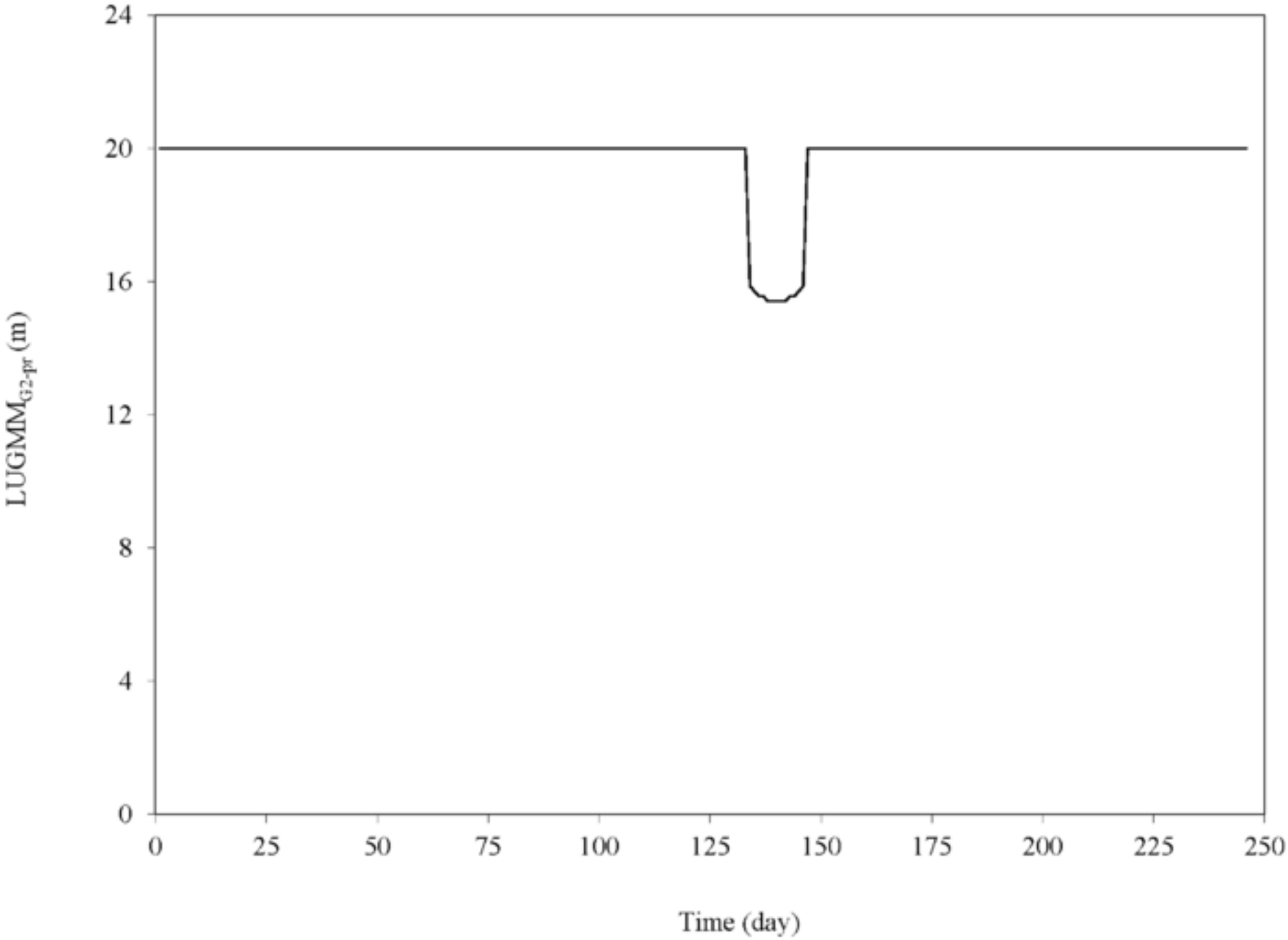
24
20
16
12
8
4
0
LUGMM$_{G2\text{-}pr}$ (m)
0
25
50
75
100
125
150
175
200
225
250
Time (day)

Figure 12a

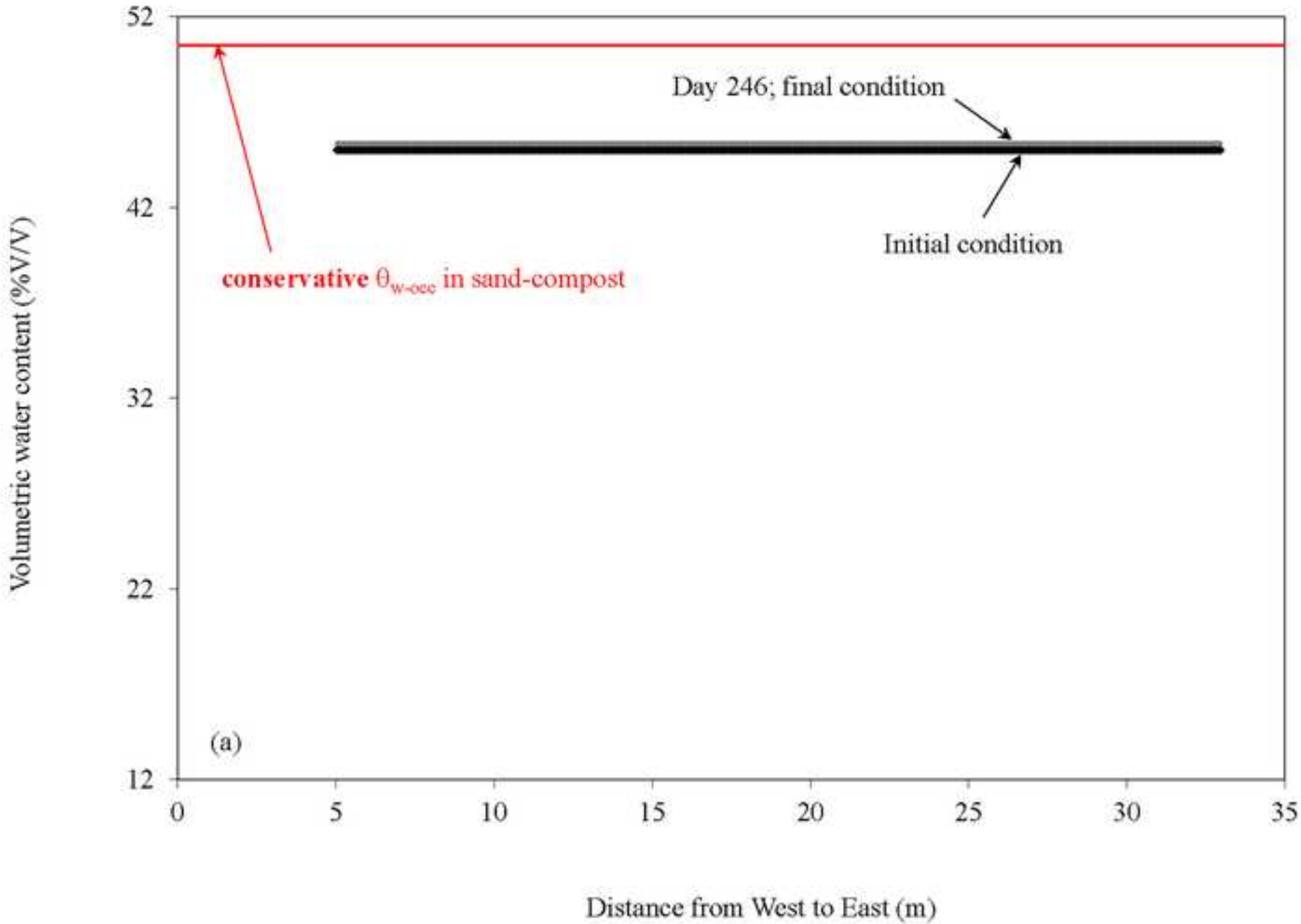
52
42
32
22
12
0
5
10
15
20
25
30
35
Volumetric water content (%V/V)
Distance from West to East (m)
Day 246; final condition
Initial condition
conservative θw-occ in sand-compost
(a)

Figure 12b

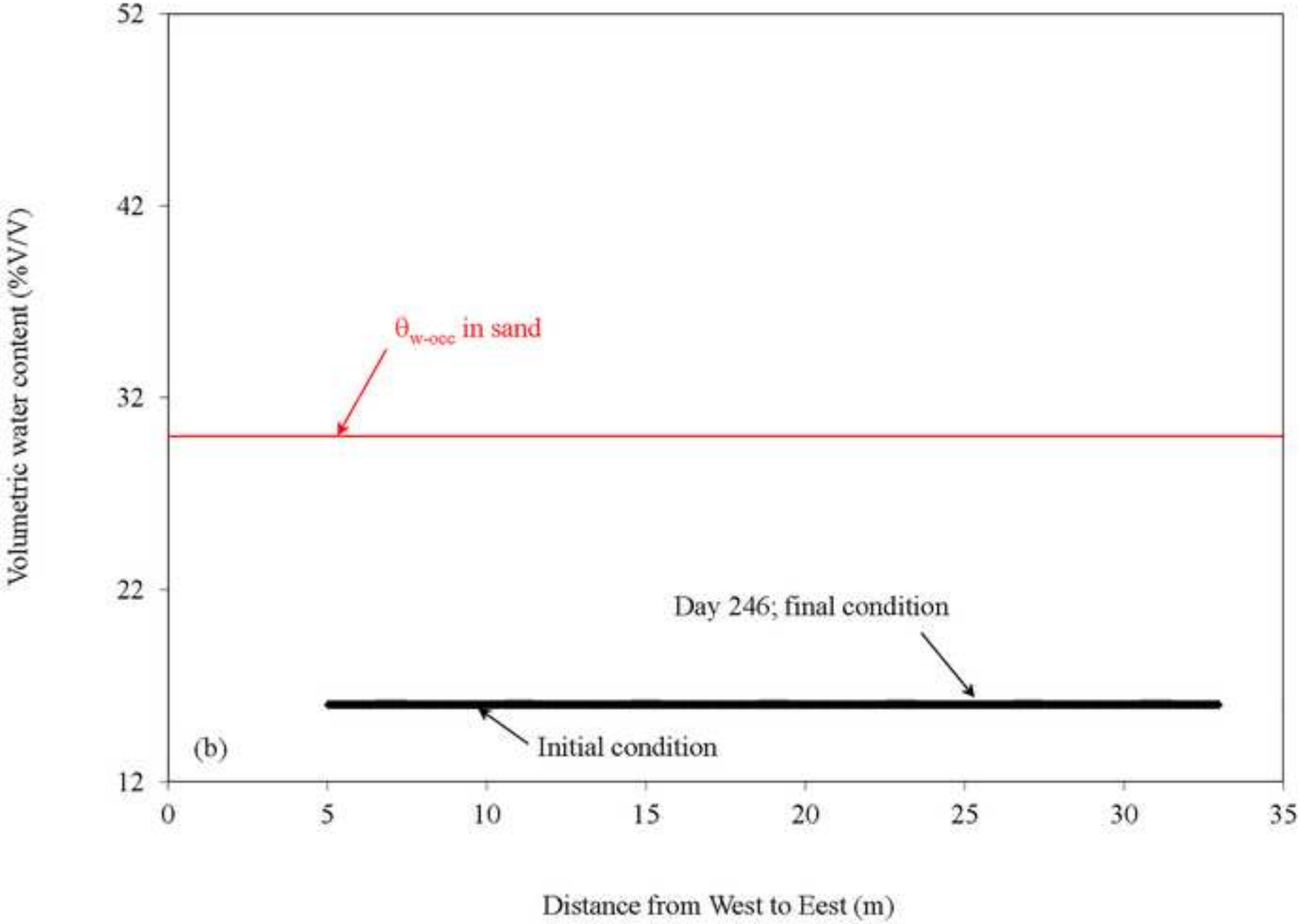
52
42
32
22
12
Volumetric water content (%V/V)
θw-occ in sand
Day 246; final condition
Initial condition
(b)
0
5
10
15
20
25
30
35
Distance from West to Eest (m)

Figure 13a

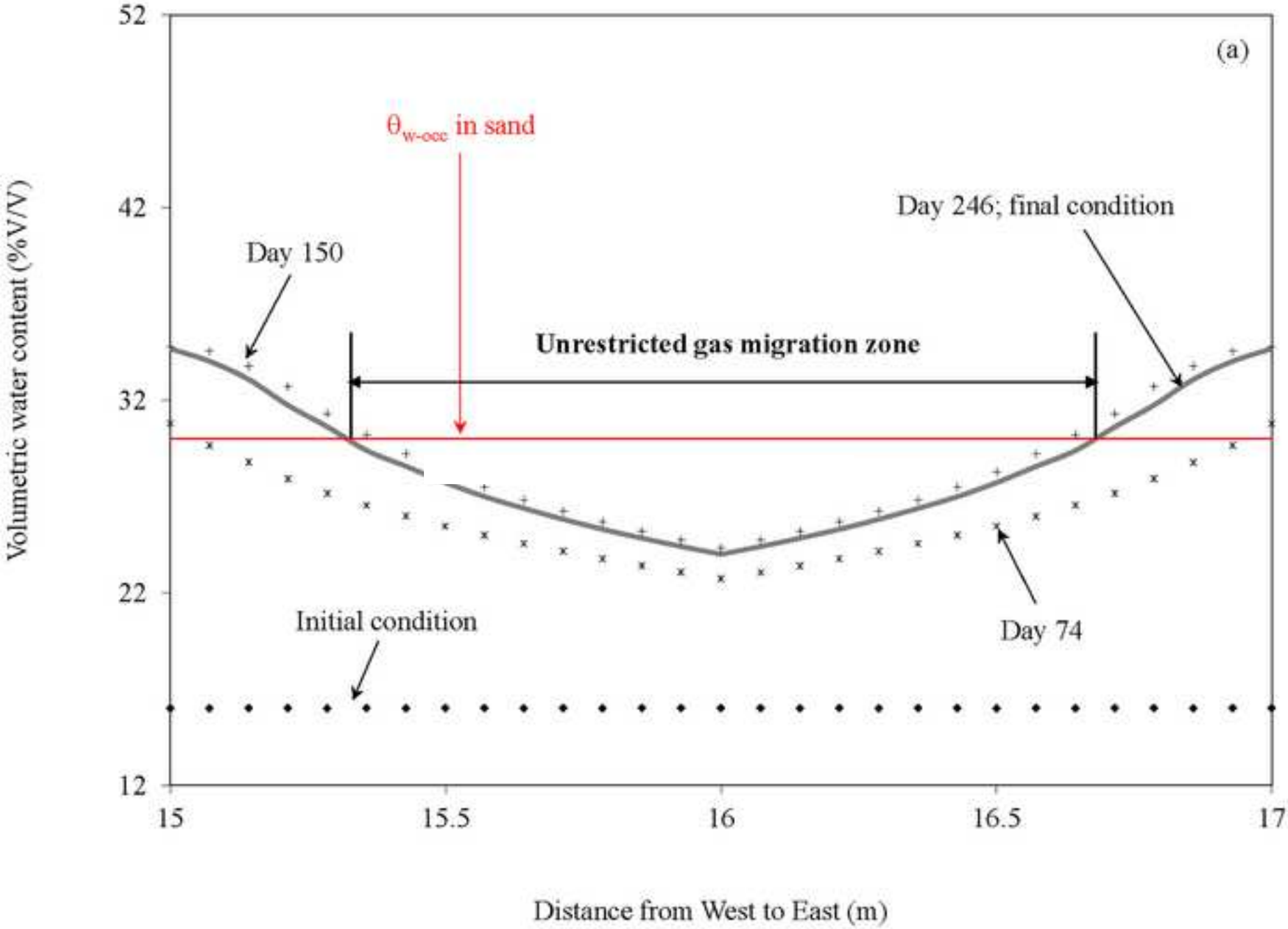
(a)
$\theta_{w\text{-}occ}$ in sand
Day 150
Day 246; final condition
Unrestricted gas migration zone
Initial condition
Day 74
Volumetric water content (%V/V)
52
42
32
22
12
15
15.5
16
16.5
17
Distance from West to East (m)

Figure 13b

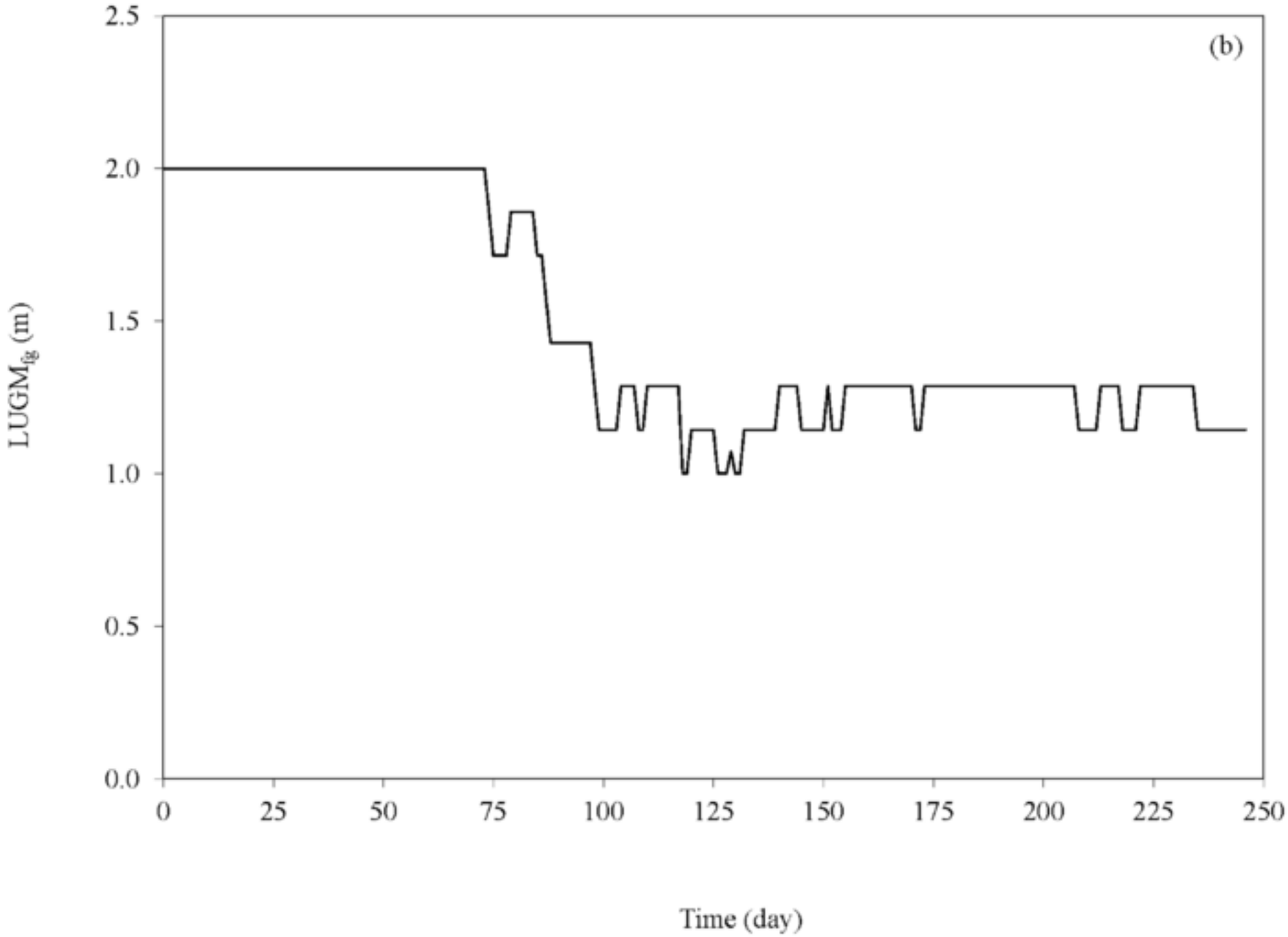
(b)
2.5
2.0
1.5
1.0
0.5
0.0
LUGM$_{fg}$ (m)
0
25
50
75
100
125
150
175
200
225
250
Time (day)

Figure 14a

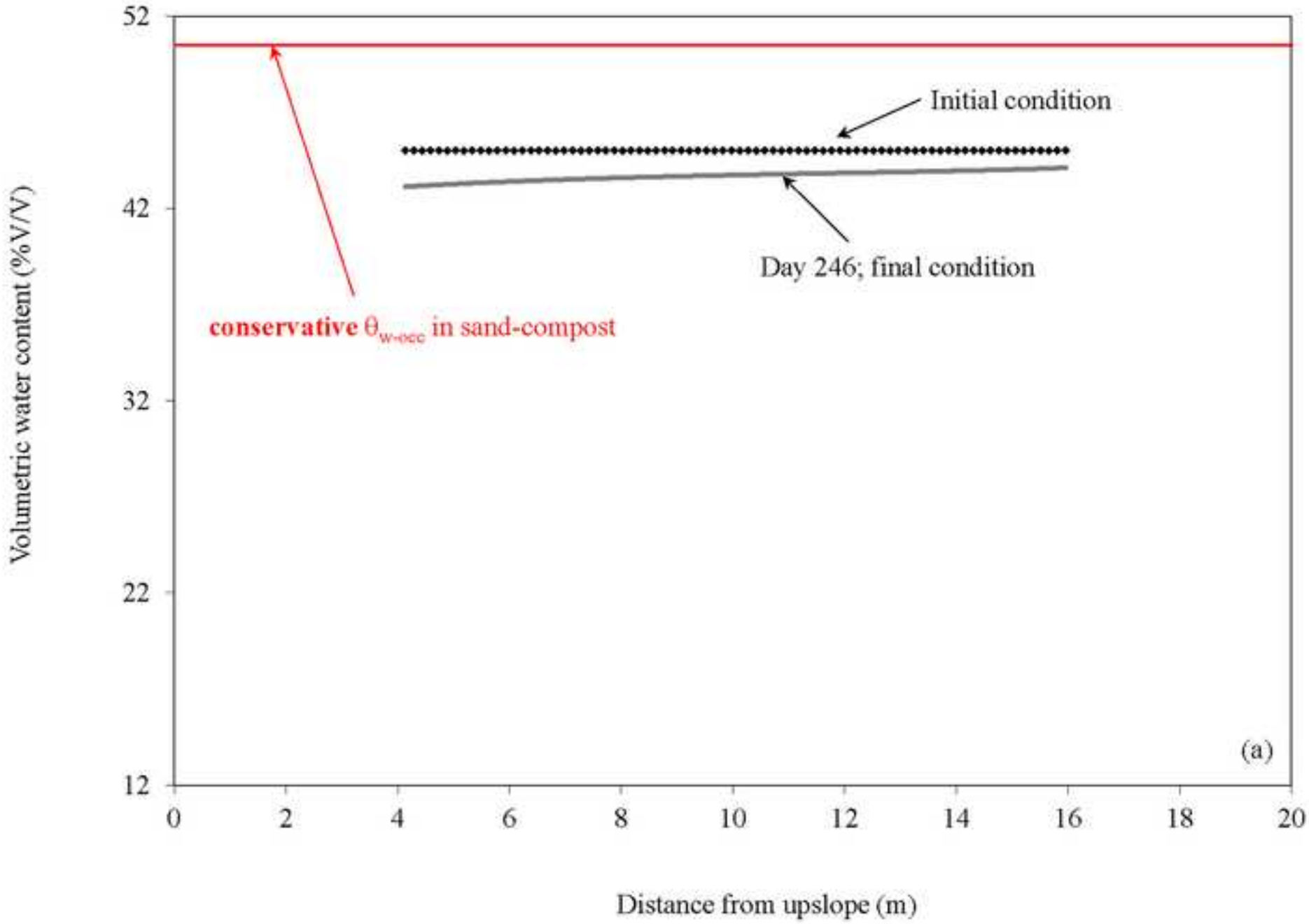
52
42
32
22
12
Volumetric water content (%V/V)
Initial condition
Day 246; final condition
conservative $\theta_{w\text{-}occ}$ in sand-compost
(a)
0
2
4
6
8
10
12
14
16
18
20
Distance from upslope (m)

Figure 14b

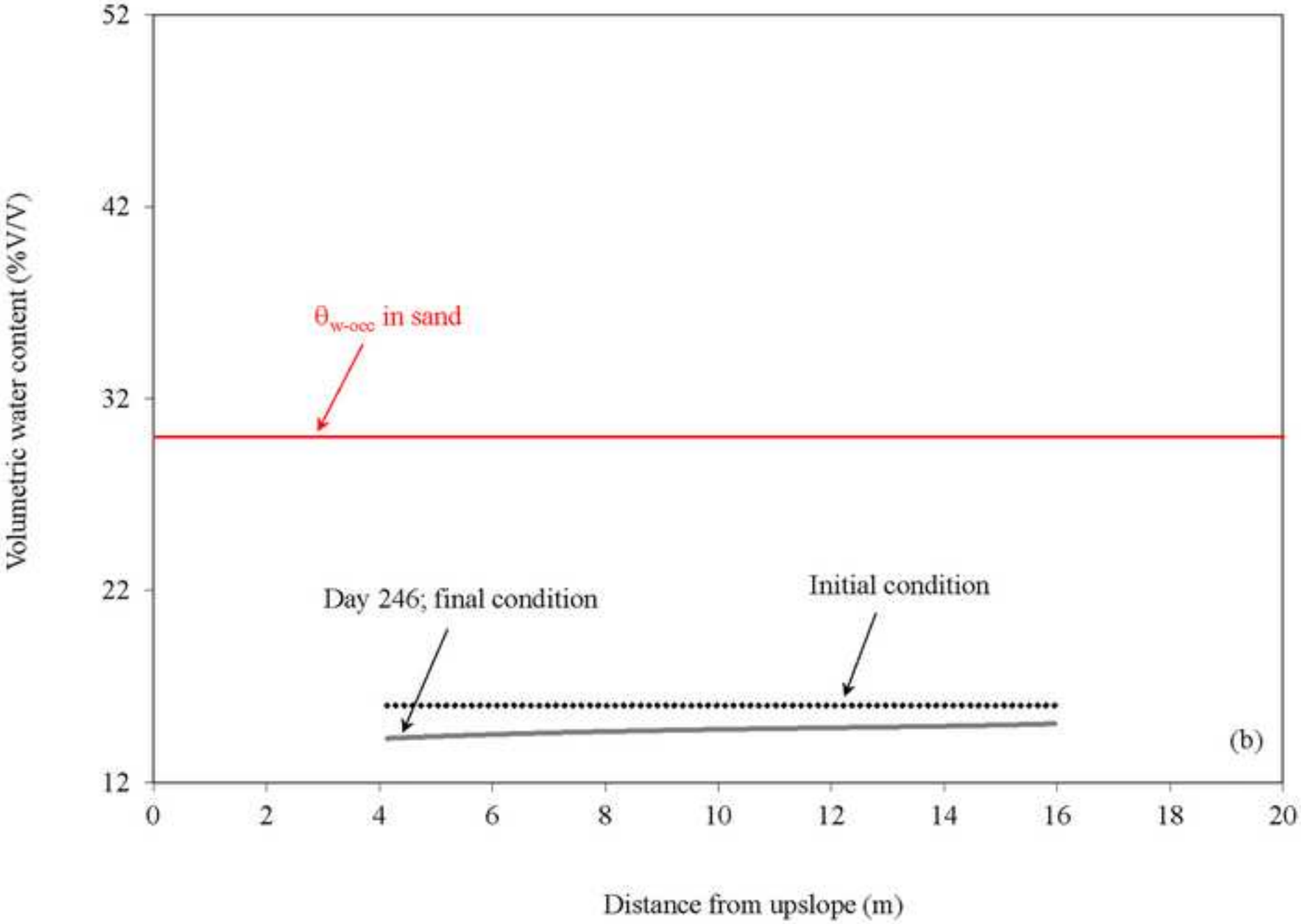
52
42
32
22
12
Volumetric water content (%V/V)
θw-occ in sand
Day 246; final condition
Initial condition
(b)
0
2
4
6
8
10
12
14
16
18
20
Distance from upslope (m)

Figure 15

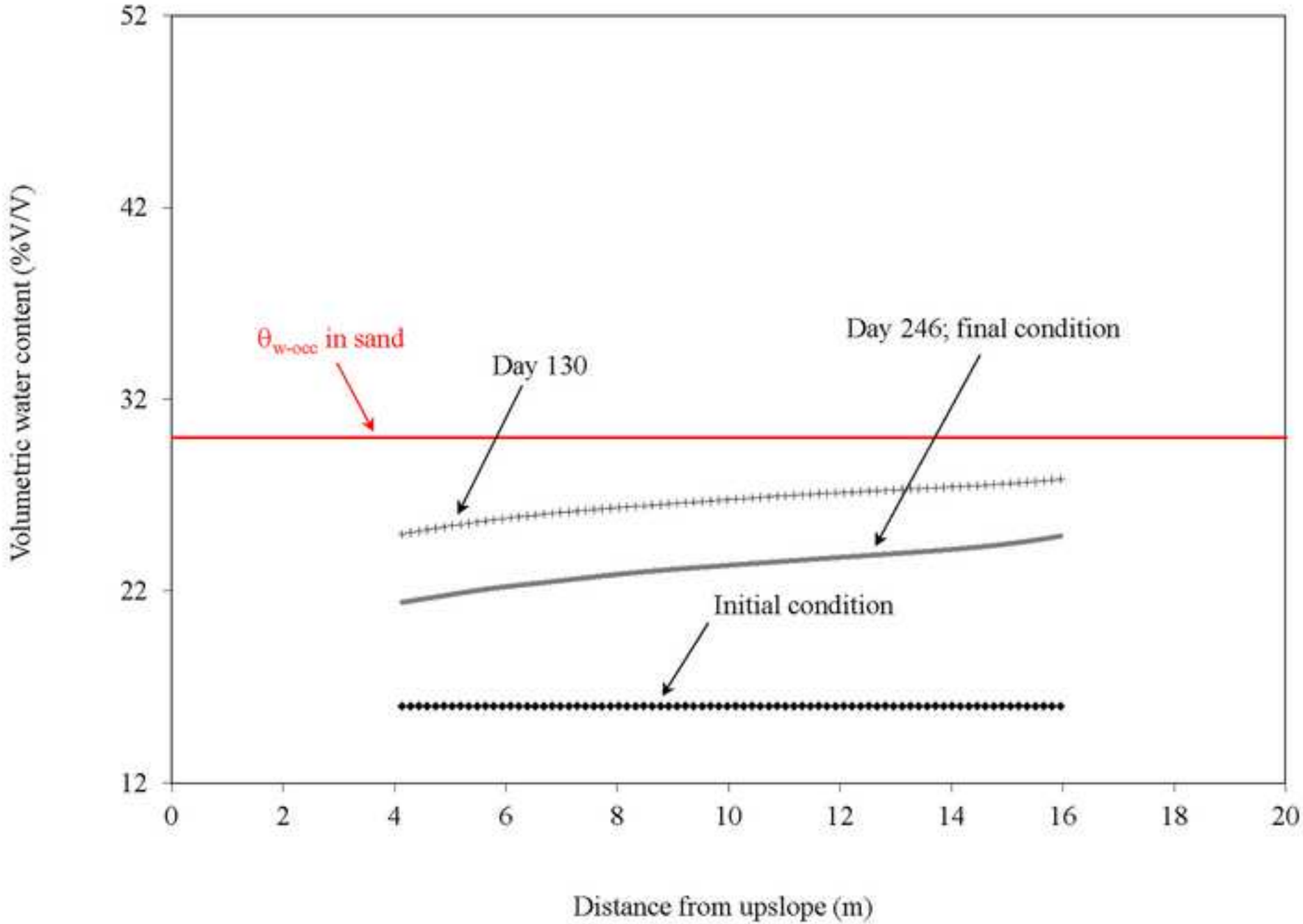
52
42
32
22
12
0
2
4
6
8
10
12
14
16
18
20
Volumetric water content (%V/V)
Distance from upslope (m)
θw-occ in sand
Day 130
Day 246; final condition
Initial condition